AD-A185 272 ACTIVE NITROGEN GENERATION(U) MCDONNELL DOUGLAS 1/1
RESEARCH LABS ST LOUIS MO P D WHITEFIELD ET AL. JUN 87
AFWL-TR-86-61 F29601-84-C-0075

UNCLASSIFIED F/G 7/2 NL

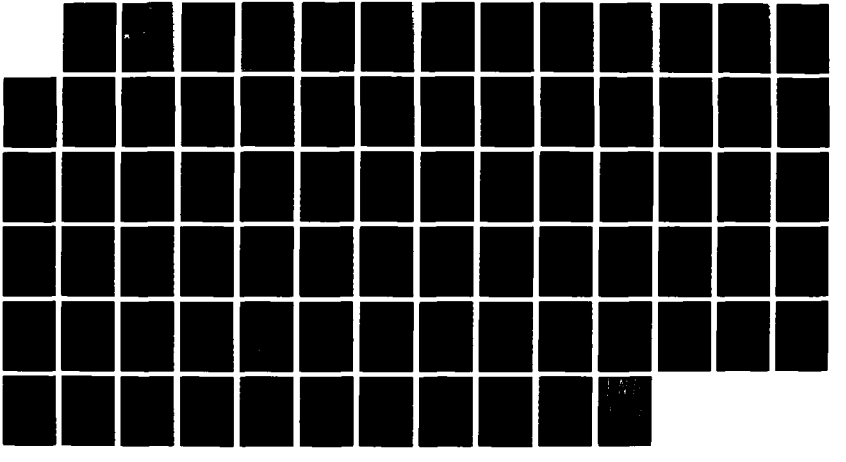

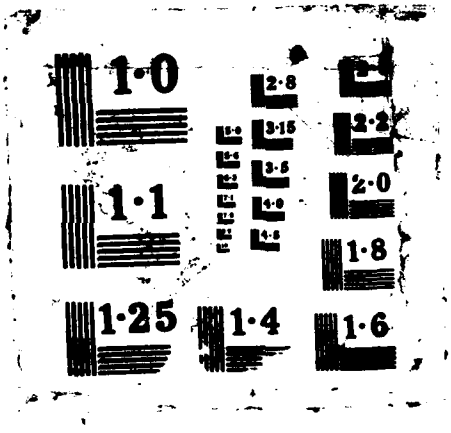
1·0
1·1
1·25
2·8
3·15
3·5
4·0
1·4
2·2
2·0
1·8
1·6

AFWL-TR-
86-61

ACTIVE NITROGEN GENERATION

P. D. Whitefield
F. E. Hovis

McDonnell Douglas Research Laboratories
St Louis, MO 63166

June 1987

Final Report

Approved for public release; distribution unlimited.

AIR FORCE WEAPONS LABORATORY
Air Force Systems Command
Kirtland Air Force Base, NM 87117-6008

This final report was prepared by McDonnell Douglas Research Laboratories, St Louis, Missouri, under Contract F29601-84-C-0075, Job Order 33261W13 with the Air Force Weapons Laboratory, Kirtland Air Force Base, New Mexico. First Lieutenant Brian D. McFeeters (ARDA) was the Laboratory Project Officer-in-Charge.

When Government drawings, specifications, or other data are used for any purpose other than in connection with a definitely Government-related procurement, the United States Government incurs no responsibility or any obligation whatsoever. The fact that the Government may have formulated or in any way supplied the said drawings, specifications, or other data, is not to be regarded by implication, or otherwise in any manner construed, as licensing the holder, or any other person or corporation; or as conveying any rights or permission to manufacture, use, or sell any patented invention that may in any way be related thereto.

This report has been authored by a contractor of the United States Government. Accordingly, the United States Government retains a nonexclusive, royalty-free license to publish or reproduce the material contained herein, or allow others to do so, for the United States Government purposes.

This report has been reviewed by the Public Affairs Office and is releasable to the National Technical Information Services (NTIS). At NTIS, it will be available to the general public, including foreign nations.

If your address has changed, if you wish to be removed from our mailing list, or if your organization no longer employs the addressee, please notify AFWL/ARDA, Kirtland AFB, NM 87117-6008 to help us maintain a current mailing list.

This technical report has been reviewed and is approved for publication.

BRIAN D. McFEETERS
1st Lt, USAF
Project Officer

FOR THE COMMANDER

GERALD A. HASEN
Major, USAF
Chief, Advanced Chemical Laser Br

HARRO ACKERMANN
Lt Col, USAF
Chief, Laser Science & Technology Ofc

DO NOT RETURN COPIES OF THIS REPORT UNLESS CONTRACTUAL OBLIGATIONS OR NOTICE ON A SPECIFIC DOCUMENT REQUIRES THAT IT BE RETURNED.

REPORT DOCUMENTATION PAGE

1a. REPORT SECURITY CLASSIFICATION: UNCLASSIFIED	1b. RESTRICTIVE MARKINGS
2a. SECURITY CLASSIFICATION AUTHORITY	3. DISTRIBUTION/AVAILABILITY OF REPORT: Approved for public release; distribution unlimited.
2b. DECLASSIFICATION/DOWNGRADING SCHEDULE	
4. PERFORMING ORGANIZATION REPORT NUMBER(S)	5. MONITORING ORGANIZATION REPORT NUMBER(S): AFWL-TR-86-61
6a. NAME OF PERFORMING ORGANIZATION: McDonnell Douglas Research Laboratories; 6b. OFFICE SYMBOL (If applicable)	7a. NAME OF MONITORING ORGANIZATION: Air Force Weapons Laboratory
6c. ADDRESS (City, State and ZIP Code): McDonnell Douglas Corporation, St Louis, Missouri 63166	7b. ADDRESS (City, State and ZIP Code): Kirtland Air Force Base, NM 87117-6008
8a. NAME OF FUNDING/SPONSORING ORGANIZATION; 8b. OFFICE SYMBOL (If applicable)	9. PROCUREMENT INSTRUMENT IDENTIFICATION NUMBER: F29601-84-C-0075
8c. ADDRESS (City, State and ZIP Code)	10. SOURCE OF FUNDING NOS.

PROGRAM ELEMENT NO.	PROJECT NO.	TASK NO.	WORK UNIT NO.
62601F	3326	1W	13

11. TITLE (Include Security Classification): ACTIVE NITROGEN GENERATION

12. PERSONAL AUTHOR(S): Whitefield, P.D.; and Hovis, F.E.

13a. TYPE OF REPORT	13b. TIME COVERED	14. DATE OF REPORT (Yr., Mo., Day)	15. PAGE COUNT
Final	FROM 24Sep84 TO 24Mar86	1987 June	80

16. SUPPLEMENTARY NOTATION

17. COSATI CODES			18. SUBJECT TERMS (Continue on reverse if necessary and identify by block number)
FIELD	GROUP	SUB. GR.	Chemical lasers Spectroscopy Active nitrogen Kinetics
20	05		

19. ABSTRACT (Continue on reverse if necessary and identify by block number)

The following measurements have been made:

a. The absolute population of $N_2(A)$, $N_2(B)$, and $NF(a^1\Delta)$ produced in the $H/H_2 + NF_2$ flame.

b. A comparison of the efficiencies of production for the above species was made in the $D + NF_2$ flame, where no D_2 was present.

c. The room temperature rate constants for the reactions:

(1) $N(^2D) + O_2 \rightarrow NO + O$; $k = (6.6 \pm 1.0) \times 10^{-12}$ cm^3 s^{-1}

(2) $N(^2D) + H_2 \rightarrow$ Products; $k = (1.8 \pm 0.8) \times 10^{-12}$ cm^3 s^{-1}

20. DISTRIBUTION/AVAILABILITY OF ABSTRACT	21. ABSTRACT SECURITY CLASSIFICATION
UNCLASSIFIED/UNLIMITED ☒ SAME AS RPT. ☐ DTIC USERS []	UNCLASSIFIED

22a. NAME OF RESPONSIBLE INDIVIDUAL	22b. TELEPHONE NUMBER (Include Area Code)	22c. OFFICE SYMBOL
Lt Brian D. McFeeters	(505) 844-0883	ARDA

19. ABSTRACT (Continued)

(3) $N(^2D) + HF \rightarrow$ Products; $k = (1.0 \pm 0.3) \times 10^{-12}$ cm^3 s^{-1}

(4) $N(^2D) + NF(a) \quad N_2(B,W) + F$; $k = 1.0 \times 10^{-10}$ cm^3 s^{-1}

(5) $N_2(A) + H \rightarrow$ Products; $k = (5.1 \pm 1.5) \times 10^{-11}$ cm^3 s^{-1}

Reactions a-d were measured in a fast flow reactor equipped with an atomic resonance absorption experiment to monitor $N(^2D)$ atoms. Reactions a-c were measured under pseudo-first order kinetic conditions where the molecular reactants were in excess (i.e., $[N(^2D)] << [O_2, H_2, \text{ or } HF]$. The rate constant for reaction d was measured by performing a steady-state analysis of $N_2(B,W)$ production and loss in the $H + NF_2$ flame (i.e., assuming $d[N_2(B,W)]/dt \simeq 0$). Reaction e was studied in the OES reaction under pseudo-first order conditions where $[N_2(A)] << [H]$.

The report is concluded with a discussion of the impact on the foregoing results on the current understanding of the mechanism of $N_2(A)$ production in the $H + NF_2$ flame and an evaluation of the $H + NF_2$ flame as a potential $N_2(A)$ generator for a high energy chemical laser.

SUMMARY

This report presents the results of an evaluation of the H + NF_2 flame as an efficient generator of electronically excited molecular nitrogen (Active Nitrogen). To this end, the following measurements have been made:

(1) The absolute populations of ($N_2(A)$, $N_2(B)$, and $NF(a^1\Delta)$) produced in the H/H_2 + NF_2 flame were measured. This work was performed in a fast-flow reactor equipped with an optical emission spectroscopy (OES) experiment. Hydrogen atoms were generated by a microwave discharge in a dilute mixture of H_2 in He or Ar.

(2) A comparison of the efficiencies of production for these species was made for the D + NF_2 flame, in which no D_2 was present. This work was also performed in the OES flow reactor. In this case, the D atoms were generated in the complete reaction of F + D_2 → DF + D. This chemical D-atom generation technique was precalibrated in another fast-flow reactor equipped with gas-phase electron paramagnetic resonance (EPR) diagnostics.

(3) The room-temperature rate constants were measured for the following reactions:

a. $N(^2D) + O_2 \rightarrow NO + O$; $k = (6.6 \pm 1.0) \times 10^{-12}$ cm^3 s^{-1}
b. $N(^2D) + H_2 \rightarrow$ Products; $k = (1.8 \pm 0.8) \times 10^{-12}$ cm^3 s^{-1}
c. $N(^2D) + HF \rightarrow$ Products; $k = (1.0 \pm 0.3) \times 10^{-12}$ cm^3 s^{-1}
d. $N(^2D) + NF(a) \rightarrow N_2(B,W) + F$; $k = 1.0 \times 10^{-10}$ cm^3 s^{-1}
e. $N_2(A) + H \rightarrow$ Products; $k = (5.1 \pm 1.5) \times 10^{-11}$ cm^3 s^{-1}

Reactions a-d were measured in a fast-flow reactor equipped with an atomic-resonance absorption device to monitor $N(^2D)$ atoms. Reactions a-c were measured under pseudo-first-order kinetic conditions of excess molecular reactants (i.e., $[N(^2D)] \ll [O_2, H_2, \text{or HF}]$). The rate constant for reaction d was measured by performing a steady-state analysis of $N_2(B,W)$ production and loss in the H + NF_2 flame (i.e., assuming $d[N_2(B,W)]/dt = 0$). This study required the simultaneous determination of absolute concentrations of $N(^2D)$, NF(a), and $N_2(B)$ in the H + NF_2 flame under given stoichiometric conditions.

Reaction e was studied in the OES reactor under pseudo-first-order conditions where $[N_2(A)] \ll [H]$.

The report concludes with a discussion of the impact of the foregoing results on the current understanding of the mechanism of $N_2(A)$ production in the $H + NF_2$ flame and an evaluation of the $H + NF_2$ flame as a potential Active Nitrogen Generator for a high-energy chemical laser.

CONTENTS

CONTENTS (Continued)

ILLUSTRATIONS

ILLUSTRATIONS (Continued)

LIST OF TABLES

I. INTRODUCTION

This report describes measurements of the absolute production efficiencies of $N_2(B)$ under optimum stoichiometric conditions and the experimental determinations of the rate constants for four key processes in the $H + NF_2$ generation mechanism, three of which are original measurements. McDonnell Douglas Research Laboratories (MDRL) has applied the following experimental techniques to this effort.

(1) optical emission spectroscopy (OES);

(2) atomic resonance spectrometry;

(3) electron paramagnetic resonance (EPR) spectrometry; and

(4) modulated molecular beam mass spectrometry.

Results of this study have significantly enhanced the understanding of $N_2(A)$ production in the $H + NF_2$ scheme and lead to several recommendations for continued research to resolve key issues.

II. BACKGROUND

This section summarizes the salient background information published before this study and used to identify its key tasks.

The reaction of H atoms with NF_2 radicals produces metastable $NF(a^1\Delta)$ radicals and vibrationally excited HF[v(vibrational quantum number) $\leq$ 3] as primary products.

$$H + NF_2 \rightarrow HF + NF \qquad (1)$$

The rate constant for reaction (1) has been measured to be $(1.5 \pm 0.2) \times 10^{-11}$ $cm^3\ s^{-1}$, with a branching ratio of 0.9 for the $NF(a^1\Delta)$ product (Refs. 1-3). This reaction initiates a series of highly exothermic secondary reactions producing such species as $N(^2D)$, $N(^2P)$, $N(^4S)$, $F(^2P)$, $NF(b^1\Sigma^+)$, $NF(a^1\Delta)$, $NF(X^3\Sigma^-)$, $N_2(B^3\Pi_g)$, $N_2(A^3\Sigma_u^+)$, $N_2(a^1\Pi_g)$, $N_2(X^1\Sigma^+_g)$, $NH(c^1\Pi)$, $NH(a^1\Delta)$, $NH(A^3\Pi)$, and $NH(X^3\Sigma^-)$. All have been identified spectroscopically from either optical emissions and atomic resonance spectrometry or have had their presence inferred since they are the terminating levels for detected emissions (Refs. 1-6). Table 1 is a list of the species, their spectroscopic assignments, and the stoichiometric conditions under which these reactions have been detected in the $H + NF_2$ flame.

The $N_2(A^3\Sigma_u^+)$ state is metastable with a radiative lifetime $\tau_{rad} = 2$ s and electronic energy $T_e(A^3\Sigma_u^+) = 50203.6\ cm^{-1}$ (Ref. 7). The lifetime and electronic energy of $N_2(A^3\Sigma_u^+)$ molecules and their chemical production in the $H + NF_2$ flame makes them eligible as energy storage/transfer partners for a high-energy chemical laser device. The $N_2(A^3\Sigma_u^+)$ molecule has the potential to transfer so much energy in one step ($\approx$ 6 times that transferred by an $O_2(a^1\Delta)$ molecule) that an extensive range of lasing species can be considered. Use of these species in a laser device, however, is predicated on the the development of an efficient $N_2(A)$ production scheme.

Little is known about the efficiency of $N_2(A)$ production in the $H + NF_2$ flame. From the available data, a series of important reaction sequences for $N_2(A)$ production can be established. These sequences are presented schematically in Figure 1. The background to each sequence is summarized as follows.

TABLE 1. COMPILATION OF DATA PUBLISHED ON SPECIES PRODUCED IN THE $H + NF_2$ SYSTEM (AS OF APRIL 1984)

Species	Transitions and Wavelengths Observed	Required Stoichiometry for Observation	Measurement Techniques	Ref
$NF(a^1\Delta)$	$NF(a^1\Delta - X^3\Sigma^-)$ ~874 nm 0–0 band	All conditions	OES	1,2 4
$NF(b^1\Sigma^+)$	$NF(b^1\Sigma^+ - X^3\Sigma^-)$ 524-528 nm 0–0, 1–1, 2–2, 3–3 and 4–4 bands	All conditions	OES	4 5
$HF(v \leq 4)$	IR to Visible	All conditions	OES	4
$N(^2D)$	$N(^2P - ^2D)$ 149.3 nm	$[H] > [NF_2]$	ARF	2
$N(^2P)$	$N(^2P - ^2P)$ 174.3 nm	$[H] > [NF_2]$	ARF	2
$N(^4S)$	$N(^4P - ^4S)$ 120.0 nm	$[H] > [NF_2]$	ARF	2
$N_2(B^3\pi_g)$	$N_2(B^3\pi_g - A^3\Sigma^+_u)$ 650–880 nm	$[H] > [NF_2]$	OES	4
$N_2(A^3\Sigma^+_u)$	inferred from lower level of B-A emission			
$N_2(a^1\pi_g)$	$N_2(a^1\pi_g - X^1\Sigma^+_g)$ 140 – 180 nm	$[H] > [NF_2]$	OES	4
$N_2(a'^1\Sigma^-_u)$	$N_2(a'^1\Sigma^-_u - X^1\Sigma^+_g)$ 140–180 nm	$[H] > [NF_2]$	OES	4
$NH(c^1\pi)$	$(NH(c^1\pi - a^1\Delta)$ 326 nm	$[H] > [NF_2]$	OES	4
$NH(a^1\Delta)$	inferred as lower level of NH(c–a)			
$NH(A^3\pi)$	$NH(A^3\pi - X^3\Sigma^-)$ 336 nm	$[H] > [NF_2]$	OES	4

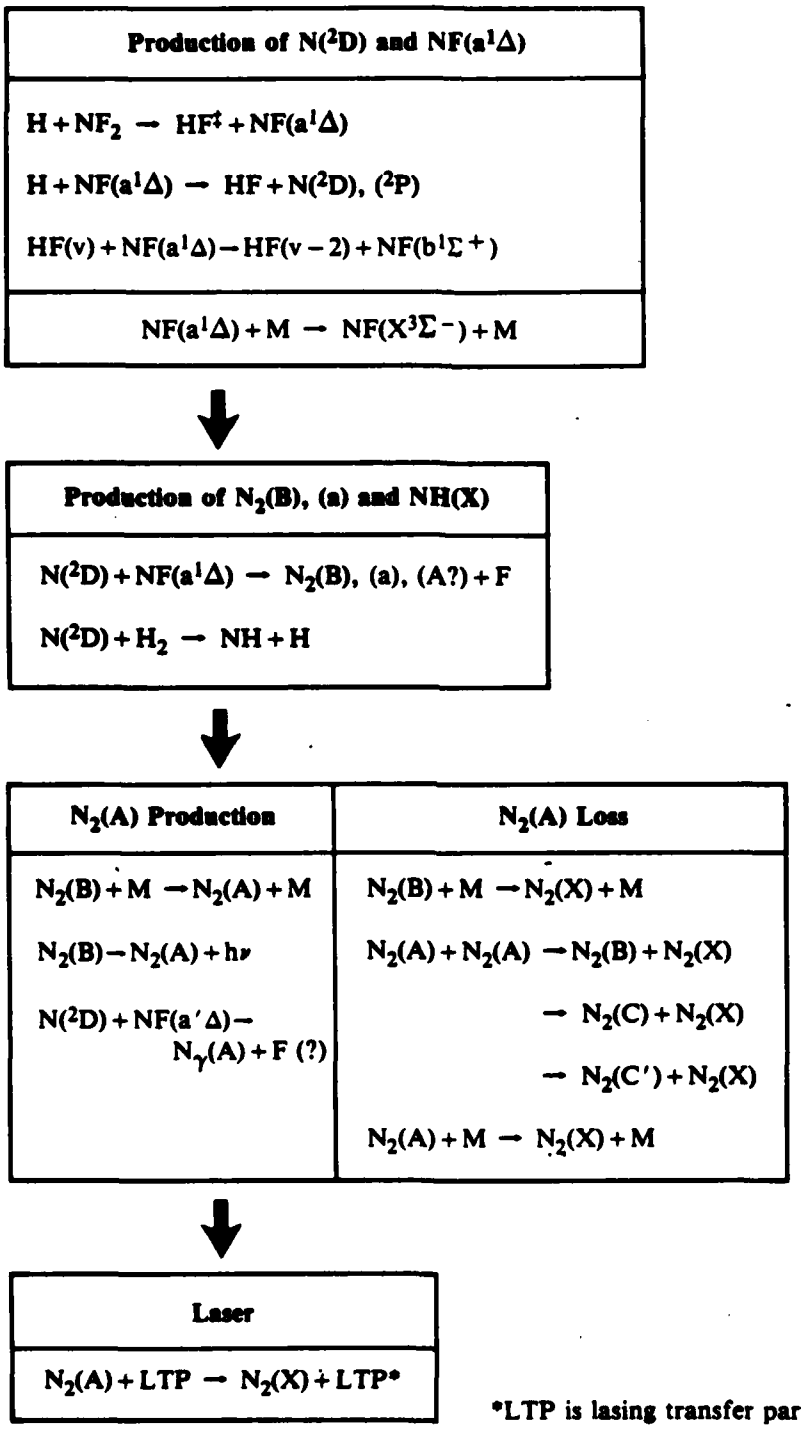

Figure 1. Important reaction sequences for $N_2(A)$ production in the $H + NF_2$ system.

1. PRODUCTION OF $N(^2D)$ AND $NF(a^1\Delta)$

The rate constant and branching ratio of the $NF(a^1\Delta)$ product for reaction (1) and the metastability of $NF(a^1\Delta)$, (τ_{rad} = 5.6 (± 50%) s) (Ref. 3), indicate that $NF(a^1\Delta)$ will dominate secondary reactive processes in the H + NF_2 flame. With $[H]_o > [NF_2]_o$, the production of metastable $N(^2D)$ atoms, and to a lesser extent $N(^2P)$ atoms, has been observed and monitored with atomic resonance fluorescence spectrometry (Refs. 2 and 4). Reaction (2) has been proposed as the source of excited nitrogen atom in this system and a rate constant of 2.5 x 10^{-13} cm^3 s^{-1} has been estimated (Ref. 1) for this reaction.

$$H + NF(a^1\Delta) \rightarrow N(^2D), (^2P) + HF \qquad (2)$$

Such a rate constant would account for significant reactive depletion of $NF(a^1\Delta)$. The major depletion of $NF(a^1\Delta)$, however, is attributed to electronic quenching by molecular species in the reactive flow

$$NF(a^1\Delta) + M \rightarrow NF(X^3\Sigma^-) + M \qquad (3)$$

where M = H_2, HF, NF_2, etc.)

If unreacted H_2 is present in the reactive flow, large quantities of HF(v ≤ 3) will be generated due to the reaction of H_2 with F atoms (Ref 1). Efficient V-E energy transfer from HF to $NF(a^1\Delta)$, producing $NF(b^1\Sigma^+)$, has been reported as the reaction (Ref. 5)

$$NF(a^1\Delta) + HF(v) \rightarrow NF(b^1\Sigma^+) + HF(v-2) \qquad (4)$$

Thus, the presence of unreacted H_2 opens another depletion channel for $NF(a^1\Delta)$. However, this channel can be minimized by substituting H_2 with D_2 in the reactive flow, since reduction of $NF(b^1\Sigma^+)$ emission intensity has been reported when D_2 was used (Ref. 5).

2. PRODUCTION OF $N_2(B^3\Pi_g)$, $N_2(a^1\Pi_g)$, and $NH(X^3\Sigma^-)$

When [H] > $[NF_2]$, N_2 electronic emissions from the $B^3\Pi_g$ and $a^1\Pi_g$ states are observed and the $c^1\Pi$, $a^1\Delta$, and $A^3\Pi$ states of NH are observed. The time evolution of these species is reported to follow quantitatively those of $N(^2D)$ and $NF(a^1\Delta)$ (Ref. 4). Reference 4 further reported that the N_2 first positive

band emission (N_2(B-A) emission) varies in direct proportion with the product $[N(^2D)] \times [NF(a^1\Delta)]$. These results are consistent with the postulation that the electronically excited N_2 precursor reaction in the H + NF_2 flame must be the highly exothermic reaction of $N(^2D)$ atoms with $NF(a^1\Delta)$ (Ref. 6) as follows:

$$N(^2D) + NF(a^1\Delta) \rightarrow N_2 + F; \quad \Delta H = -1000 \text{ kJ mole}^{-1} \tag{5}$$

The exoergicity of reaction (5) appears as electronic excitation in the N_2 product. The $N_2(B^3\Pi_g)$ $v \leq 12$, $\Delta E = 78{,}700$ cm^{-1}, and $N_2(a^1\Pi_g)$ $v \leq 2$, $\Delta E = 72{,}750$ cm^{-1} are observed in the H + NF_2 flame (Ref. 4). A collision efficiency of 0.1 has been estimated for reaction (5) to account for the extremely high intensity of the N_2(B-A) emission reported (Ref. 4). The precursor reaction for NH electronic emission is most likely to be the reaction of $N(^2D)$ atoms with H_2 (Ref. 4) as

$$N(^2D) + H_2 \rightarrow NH(X^3\Sigma^-) + H \tag{6}$$

Justification for this suggested reaction is the observation that when D_2 is used to replace H_2 in the H + NF_2 system, analagous ND emissions are observed. There have been several rate-constant measurements for reaction (6) (Refs. 8-10). This data was critically evaluated (Ref. 11) and a value of $(2.2 \pm 0.8) \times 10^{-12}$ cm^3 s^{-1} was recommended. Thus, in an H_2-rich reactive flow, reaction (6) will represent a significant loss channel for $N(^2D)$ atoms.

3. PRODUCTION AND LOSS OF $N_2(A^3\Sigma_u^+)$

The production of metastable $N_2(A^3\Sigma_u^+)$ in the H + NF_2 flame is inferred from the strong N_2(B-A) first positive band emission observed under excess H_2 reaction conditions (Ref. 1). To the best of our knowledge, prior to the study described in this final report, no direct detection of $N_2(A^3\Sigma_u^+)$ molecules has been made in the H + NF_2 flame. Optical emission from the weak A-X transitions (Vegard-Kaplan bands) was probably masked by other more intense NH emissions in the spectral regions. Radiative loss of N_2(A) to the N_2(X) ground state will not be important, considering the metastability of N_2(A). Thus, under conditions in which wall losses can be eliminated or minimized,

the dominant loss channel for $N_2(A)$ will be collisional deactivation (reaction 7) and energy pooling (reaction 8)

$$N_2(A) + M \rightarrow N_2(X) + M \quad (7)$$

$$2N_2(A) \rightarrow \text{products} \quad (8)$$

In such processes the transfer of energy to the collision partner may result in electronic excitation of the collision partner. It was suggested that the reaction

$$N_2(A^3\Sigma_u^+) + NH(X^3\Sigma^-) \rightarrow N_2(X^1\Sigma^+) + NH(c^1\Pi), (A^3\Pi) \quad (9)$$

is the source of $NH(c^1\Pi)$ and $(A^3\Pi)$ emission. The energy pooling of two $N_2(A)$ molecules has been investigated (Refs. 12-14), and three important branches have been identified:

$$N_2(A) + N_2(A) \rightarrow N_2(B) + N_2(X) \quad (10a)$$

$$\rightarrow N_2(C) + N_2(X) \quad (10b)$$

and

$$\rightarrow N_2(C') + N_2(X) \quad (10c)$$

Rate constants for reaction (10b) have been reported from two independent studies and are in reasonable agreement $(1.8 \pm 0.2) \times 10^{-10}$ cm^3 s^{-1} and $(2.6^{+2}_{-1}) \times 10^{-10}$ cm^3 s^{-1} (Refs. 12 and 14). In addition, the ratio of $k_{10a}:k_{10b}:k_{10c}$ has been reported to be 4.4:1.0:0.1, implying a total pooling rate of 1.4×10^{-9} cm^3 s^{-1} (Ref. 13). Such a pooling reaction will impact all $N_2(A)$ generation schemes, particularly when scalability is considered. Reaction (10) should be an excellent indicator of the pooling reactions, since the $N_2(C-B)$ transitions are highly allowed. These bands are commonly referred to as the second positive system of N_2. It is of interest to note that the observation of $N_2(C-B)$ emission was not reported in any of the spectroscopic analysis of the $H + NF_2$ flame.

4. $N(^4S)$ PRODUCTION AND THE NF + NF REACTION

The $N(^4S)$ atoms are also observed as products of the H + NF_2 flame. They do not appear to be products of any primary reactive process and are not responsible for the N_2(B-A) emission (Ref. 4) via the radiative recombination reactions

$$N(^4S) + N(^4S) + M \rightarrow N_2(B) + M \quad (11)$$

and

$$N_2(B) \rightarrow N_2(A) + h\nu \quad (12)$$

The concentration of $N(^4S)$ atoms increases slowly and monotonically with time and, in these experiments, reached a maximum after 30 ms of reaction time, unlike the concentration of $N(^2D)$ atoms which peaked at 8 ms. In a modeling study of the $N(^2D)$ and $N(^4S)$ profiles, the $N(^4S)$ formation appeared to be independent of $N(^2D)$ quenching but dependent on reaction (13),

$$H + NF(X^3\Sigma^-) \rightarrow HF + N(^4S) \quad (13)$$

An estimate of the rate constant for reaction (13) from that modeling resulted in a value similar to that for reaction (2). The $N(^4S)$ concentration will not be depleted in excess H_2 since the reaction of $N(^4S)$ atoms with H_2 is extremely endothermic (Ref. 2). Reactions (14), (15), and (16) are all highly exothermic:

$$NF(a^1\Delta) + NF(a^1\Delta) \rightarrow N_2 + 2F \quad (14)$$

$$NF(a^1\Delta) + NF(X^3\Sigma) \rightarrow N_2 + 2F \quad (15)$$

$$NF(X^3\Sigma) + NF(X^3\Sigma) \rightarrow N_2 + 2F \quad (16)$$

Thus, any or all of these reactions (14)-(16) may be important in propagating the reaction chain in the H + NF_2 flame since all are sources of F atoms (Ref. 1). Any F atoms produced in the flame can react with the unreacted H_2 via the reaction

$$F + H_2 \rightarrow HF + H \quad (17)$$

and thus regenerate H atoms. Modeling of the H + NF_2 chain reactions has resulted in an estimated rate constant for the total disproportionation reaction of NF radicals, k_{total}, where ($k_{total} = k_{14} + k_{15} + k_{16}$) of 7×10^{-11} cm^3 s^{-1} (Ref. 1).

III. POPULATION PROFILES AND EFFICIENCY MEASUREMENTS

1. INTRODUCTION

Measurements of the concentration profiles of $N_2(B)$, $N_2(A)$, NF(a), and NF(b) produced in the H(D) + NF_2 flame are described in this section. The H atoms were generated in a microwave discharge of H_2 in He. The D atoms were generated under D_2-free conditions by the reaction F + D_2 → DF + D under the proper stoichiometric conditions. From the $N_2(B)$ profiles it will be possible to extract the efficiency of $N_2(B)$ production in the H + NF_2 system. The efficiency of $N_2(B)$ production also represents the minimum efficiency of $N_2(A)$ production--an important parameter in evaluating the system for use as an $N_2(A)$ generator. The $N_2(A)$ profiles indicate the existence of a significant quenching channel for $N_2(A)$. The NF(a) and NF(b) profiles provide additional data for testing and extending the currently proposed kinetic model of the H + NF_2 system.

Optical emission spectroscopy (OES) was used to measure the population profiles of the species. By comparing the emission intensity of the species of interest to that from the O + NO system, the absolute concentrations can be determined (Refs. 15-19). The emissions from $N_2(B)$, NF(a), and NF(b) all occur in regions of significant O + NO emission, allowing a direct comparison. However, the wavelengths of $N_2(A)$ emission are shorter than the onset of the O + NO emission. An additional measurement of the relative sensitivity of the optical-detection system provides the data required to determine $N_2(A)$ populations.

2. DATA ANALYSIS

a. Use of O + NO reference emission--The emission from O + NO recombination provides a reasonably well-established reference for determining the concentration of radiating species (Refs. 15-19). For pressures above ~40 Pa, the intensity of the O + NO emission is given by

$$I_r(\lambda) = k_r(\lambda)[O][NO] \qquad (18)$$

where $I_r(\lambda)$ is the absolute intensity at the wavelength λ and $k_r(\lambda)$ the rate constant relating the intensity to the O and NO concentrations. From Equation

(18) it can be shown that the concentration of an emitting species M can be calculated from S_m, the measured intensity of M emission, and S_r, the measured O + NO reference emission intensity by the expression

$$[M] = ([O][NO]k_r/A_e)\int(S_m(\lambda)/S_r(\lambda))d\lambda \qquad (19)$$

where A_e is the effective radiative rate constant for the M transition observed, k_r is taken to be constant over the range of integration, and the integral extends over the emission band to which A_e applies.

b. <u>$N_2(B)$ vibrational distribution and production efficiencies</u>--The efficiency of $N_2(B)$ production E_B is defined as

$$E_B = \text{Total } N_2(B) \text{ produced/Total } N_2F_4 \text{ consumed} \qquad (20)$$

Since the radiative lifetimes for $N_2(B)$ vibrational levels v = 0 to v = 12 range from 4 to 8 μs, radiative losses are the dominant loss channel for $N_2(B)$ in these studies of the H + NF_2 system. This implies that

$$\text{Total } N_2(B) \text{ produced} = \text{Total } N_2(B) \text{ lost} \qquad (21)$$

$$= \int_0^{t_f} ([N_2(B)(t)]/\tau_e)dt$$

where t_f is the time for the reactions to go to completion and τ_e is the effective radiative lifetime for the $N_2(B)$ vibrational distribution produced.

To use Equation (21), the $N_2(B)$ vibrational distribution must be determined so that τ_e can be determined. The $N_2(B,v' \rightarrow A,v'')$ bands with $\Delta v = v'-v'' = 4$, 3, and 2 occur in the 560- to 800-nm region and are useful for determining the relative vibrational distribution for v = 2 to v = 12 (Ref. 7). To determine the v = 0 and v = 1 populations it is necessary to observe the $N_2(B \rightarrow A)$ $\Delta v = 1$, 0, and -1 emission bands in the 850- to 1250-nm region. For both of the spectral regions, the O + NO emission is used to correct for differences in the relative sensitivity of the detection system. The relative

populations of the $N_2(B)$ vibrational levels can be calculated from the emission spectra using

$$I_i/I_j = A_iN_i/A_jN_j \tag{22}$$

where I_k is the integrated intensity of the $N_2(B,v' = k \rightarrow A,v'')$ band, A_k is the Einstein A coefficient for that transition (Table 2), and N_k is the population in $N_2(B,v=k)$. Once the vibrational distribution of $N_2(B)$ has been established, τ_e is calculated from

$$1/\tau_e = \sum_{v=0}^{12} (f_v/\tau_v) \tag{23}$$

where f_v is the fractional population in level v and τ_v is the radiative lifetime of level v. Using τ_e, the $N_2(B)$ population profiles, and Equations (20) and (21), one can calculate the $N_2(B)$ production efficiencies.

c. $N_2(B)$ populations--As described, the concentration of $N_2(B)$ at a particular time t is needed to calculate the total $N_2(B)$ produced. This was done by comparing the $N_2(B)$ emission intensity for a particular band or group of bands to that from the reference O + NO emission, as described in paragraph 2.a. In the measurements, three different portions of the $N_2(B \rightarrow A)$ emission were used to determine $[N_2(B)]$: (1) the $\Delta v = 4$ band from $v' = 12 \rightarrow 6$, (2) the $\Delta v = 3$ band from $v' = 11 \rightarrow 5$, and (3) the $v' = 2 \rightarrow v'' = 1$ band. For each of these bands the effective radiative rate constant needed for Equation (19) is given by

$$A_e = \sum f_{v'}A_{v'} \tag{24}$$

where $A_{v'}$ is the radiative rate constant for the $v' \rightarrow v''$ component of the band and the sum extends over all v' in the band. The value for $f_{v'}$ is calculated from

$$f_{v'} = N_{v'}/\Sigma N_{v'} \tag{25}$$

with the sum extending over all v' contributing to the observed band. For the $\Delta v = 3$ and 4 bands, $k_r(\lambda)$ is taken to be 1.4×10^{-19} cm^3 s^{-1} nm^{-1}, the average

of the values reported in References 15, 16, 18, and 19. For the v' = 2 → v" = 1 band at 874 nm, the average value for $k_r(\lambda)$ is 9 x 10^{-20} cm^3 s^{-1} nm^{-1}. The values for the $A_{v'}$ were taken from Reference 7. It should be noted that the v' = 2 → v" = 1 band is overlapped by NF(a→X) emission. The deconvolution of these bands will be described in paragraph e.

d. $N_2(A)$ populations--The most useful $N_2(A \rightarrow X)$ emission lines for determining $N_2(A)$ concentrations lie in the 250- to 350-nm region (Ref. 12). Since the O + NO reference emission used in the determination of $N_2(B)$ concentrations is not a useful standard at <400 nm, another procedure must be used to measure $N_2(A)$ concentration. The procedure used was as follows:

(1) The relative sensitivity of the optical detection system from 280-550 nm was determined by use of a standard lamp.
(2) The calibration factor relating absolute emission intensity to measured signal was determined at 546 nm by use of the O + NO emission with known [O] and [NO].
(3) The relative sensitivities from step (1) and the calibration factor at 546 nm from step (2) were used to calculate the calibration factor relating 276-nm $N_2(A,v = 0) \rightarrow N_2(X,v = 6)$ emission intensity to $N_2(A,v = 0)$ population.

e. NF(a) populations--To accurately determine NF(a) concentrations from a→X emission at 874 nm, it is necessary to correct for the contribution from $N_2(B \rightarrow A)$ v' = 2 → v" = 1 emission. An empirical technique involving the following steps was employed:

(1) A pure NF(a→X) spectrum was recorded from the H + NF_2 flame with $[NF_2]_0 >> [H]_0$ and the [NF(a)] was determined with the procedure described in paragraph 2.a. The value of the O + NO radiative rate-constant at 860-880 nm is taken to be 9 x 10^{-20} cm^3 s^{-1} nm^{-1} (Refs. 15, 16, 18, and 19) and the radiative rate constant for the a→X transition is taken to be 0.18 s^{-1} (Ref. 3).
(2) A pure $N_2(B \rightarrow A)$ v' = 2 → v" = 1 reference spectrum was recorded from a microwave discharge in N_2/Ar and the $N_2(B,v = 2)$ concentration was

determined using a radiative rate constant for the transition of 6. x 10^{4} s^{-1} (Ref. 7).

(3) Least-squares analysis was used to find the linear combination of the reference spectra from steps (1) and (2) that best fits the unknown mixed spectrum.

This method has the advantage that both [NF(a)] and [N_2(B,v=2)] are determined. Since the N_2(B) vibrational distribution was determined as described in paragraph 2.b., the total N_2(B) concentration can also be obtained from these measurements.

f. NF(b) populations--The NF(b) populations were determined as described in paragraph 2.a. from the NF(b→X) emission at 529 nm. Most of the emission is expected from v' = 0 (Ref. 3) and no attempt was made to determine the relative contribution of the various v'. The radiative rate constant for the b→X transition was taken as 43 s^{-1} (Ref. 4) and that for the O + NO as 8 x 10^{-20} cm^3 s^{-1} nm^{-1} (Refs. 15, 16, 18, and 19).

3. EXPERIMENTAL APPARATUS

a. Flow system and reactive species generation--The flow system used to measure the population profile is illustrated in Figure 2. The flow tube is made of 7.6-cm-dia Pyrex coated with halocarbon wax and is pumped through 20-cm-dia PVC pipe by a 940 l/s Stokes model 615 blower backed by a 140 l/s Stokes model 412 Microvac pump. The chemical trap consists of an ~1-cm layer of soda lime on top of an ~1-cm layer of NaCl.

The N_2F_4/He mixtures used to generate the NF_2 were injected through a moveable heated injector made of either Pyrex (operating at ~230°C) or stainless steel (operating at ~200°C). These N_2F_4/He mixtures were prepared in the N_2F_4 remote handling facility (Appendix A). A thermocouple located 5 cm downstream of the observation ports was used to monitor gas temperatures. A number of ports were available for measuring pressures or injecting reagent gases such as NO or NO_2. Pressures were measured with a Baratron capacitance manometer. Tylan model FC260 flow controllers were used for measuring gas flow rates.

The H, O, or F atoms were generated in a microwave discharge of He and H_2, O_2, or F_2 at a fixed inlet port located 53 cm upstream of the observation

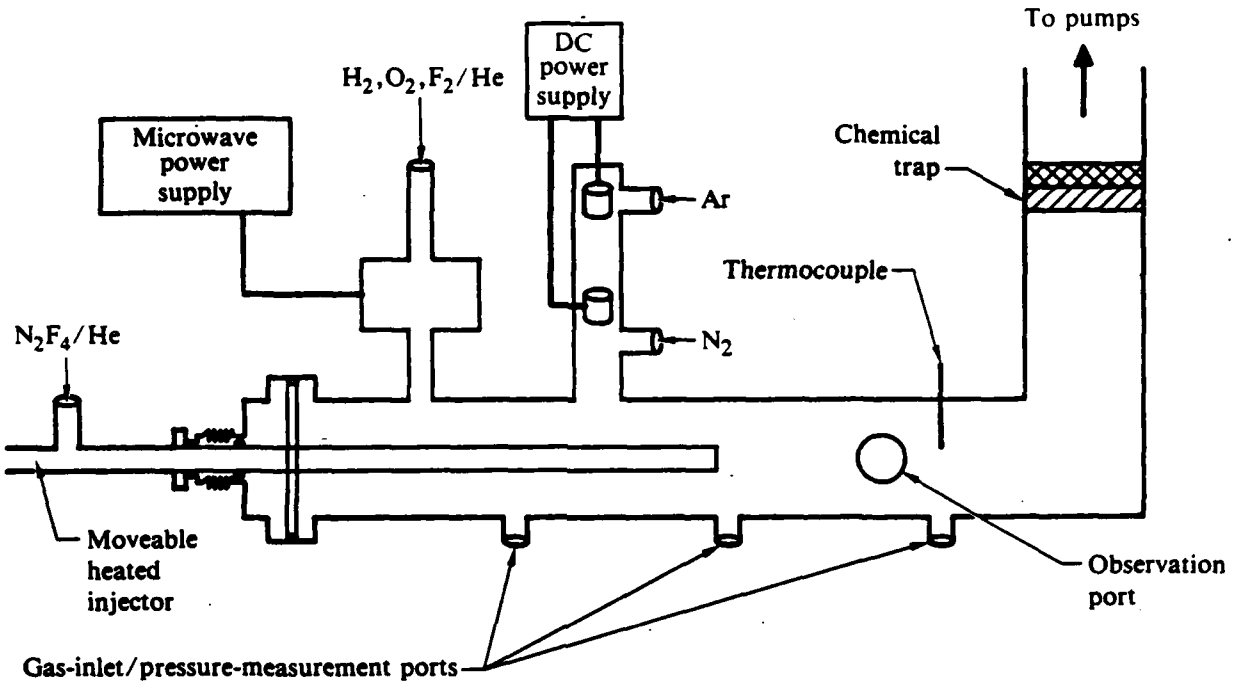

Figure 2. Flow tube used for optical emission studies.

ports. Flow conditions for $N_2(B)$, NF(a) and NF(b) profiles in the H + NF_2 flame (using an ~100-W microwave discharge in He/H_2 as the H-atom source) were 1.3 - 5.6 x 10^{18} molecules s^{-1} of H_2 in 5.8 - 6.7 x 10^{20} molecules s^{-1} of He carrier through the discharge with 2.1 - 6.1 x 10^{19} molecules s^{-1} of ~1% N_2F_4 in He through the heated injector. This gave total pressures of 80-90 Pa and flow velocities of 6.3 - 7.4 m s^{-1}. The measurements with F + D_2 as the D-atom source were performed under similar conditions except the H_2 flowing through the discharge was replaced by 5.7 x 10^{19} molecule s^{-1} of 10% F_2 in He, and 6.2 x 10^{18} molecule s^{-1} of D_2 was added ~5 cm downstream of the discharge. When O atoms were needed for the O + NO standard emission, the same basic conditions were used with 6.6 x 10^{19} molecule s^{-1} of O_2 flowing through the discharge. The O concentration was determined by the standard titration with NO_2 (Ref. 20).

For the $N_2(A)$ profiles, an additional dc discharge source for $N_2(A)$ could be added 0.38 m upstream of the observation ports. This source utilized the well-established technique of generating Ar metastables in a hollow-electrode dc discharge with subsequent transfer to N_2 to generate $N_2(A)$ (Ref.12). With the above flow system and the intensified diode array detection system, four background-corrected spectra were recorded with the extra

$N_2(A)$ source added to an H + NF_2 flame. For all four spectra the He flow through the microwave discharge was 1.5×10^{21} atoms s^{-1}, the Ar flow was 1.7×10^{21} atom s^{-1}, and the N_2 flow was 8.5×10^{20} molecules s^{-1}, yielding a total pressure of 364 Pa and a flow velocity of 9.7 m s^{-1}. When H atoms were needed, an H_2 flow of 9.0×10^{17} molecules s^{-1} was added to the He before the microwave discharge. A flow of 4.1×10^{19} molecules s^{-1} of 0.85% N_2F_4 in He could be added, either cold (no NF_2) or heated (to give NF_2), 0.14 m upstream of the observation ports.

The gases used and their purities were as follows: He, Union Carbide, 99.995%; Ar, Union Carbide, 99.997%; N_2, Air Products UHP, 99.998%; H_2, Matheson UHP, 99.999%; D_2, Air Products research grade, 99.99%; O_2, Matheson UHP, 99.99%; NO, Matheson CP, 99.0%; NO_2, Matheson CP, 99.5%; and N_2F_4 (TRW Gas Chromatographic Analysis).

b. Optical detection system and measurements--In all of the population profiles determined by OES, a PAR model 1420 intensified diode array, cooled to -25°C, was used as the detector. Acquisition and analysis of the data were performed with a PAR model 1460 OMA III console. The monochromator used to disperse the emission for these studies was a Jarrell Ash model 82-499 with a 1200-line/mm grating. The observation ports were Suprasil II. For the NF(a) measurements, a Schott RG780 long-pass glass filter prevented interference from short wavelengths transmitted in second order.

The measurements of the $N_2(B)$ vibrational distribution were performed with the flow system. All measurements were performed on the H + NF_2 flame with a microwave discharge in H_2/He as the H-atom source and with flow rates and total pressures in the ranges given. Scans of the $\Delta v = 4$, 3, and 2 visible emission bands were made with two different detection systems. The first system, providing higher resolution, incorporated a 0.5-m Jarrell Ash model 82-020 monochromator to disperse the emission and a Hamamatsu R758 photomultiplier for detection. For most of the scans a lower resolution 0.25 m Jarrell Ash model 82-410 monochromator and RCA C31034 photomultiplier were used to record the spectra. Spectra of the $\Delta v = 1$, 0, and -1 bands in the 850- to 1250-nm region were obtained with the same 0.25-m monochromator and a Northcoast model EO-817 LN_2 cooled intrinsic Ge detector. An RG780 Schott-glass filter eliminated any short-wavelength emission that could be transmitted through the monochromator in second order. The relative spectral

sensitivities needed to convert emission intensities into relative populations were determined from spectra of the O + NO reference emission.

The measurements of the relative spectral sensitivity of the intensified diode-array-based detection system needed for determining the $N_2(A)$ concentrations were made with an Eppley model EP standard lamp and a model 6162B-SR regulated power supply. In the ultraviolet (UV) measurements, the intense visible emission scattered inside the monochromator interfered with the UV signal. This interference was corrected by running background spectra with a long-pass glass filters with cut-off wavelengths longer than the wavelengths of interest.

4. RESULTS AND DISCUSSION

a. NF(a) population profiles--The results of three different NF(a) population profile measurements are shown in Figure 3. The two profiles obtained with the Pyrex injector had the same H_2 and He carrier flows and the same N_2F_4/He mixture. The only difference, was the flow rate of the N_2F_4/He,

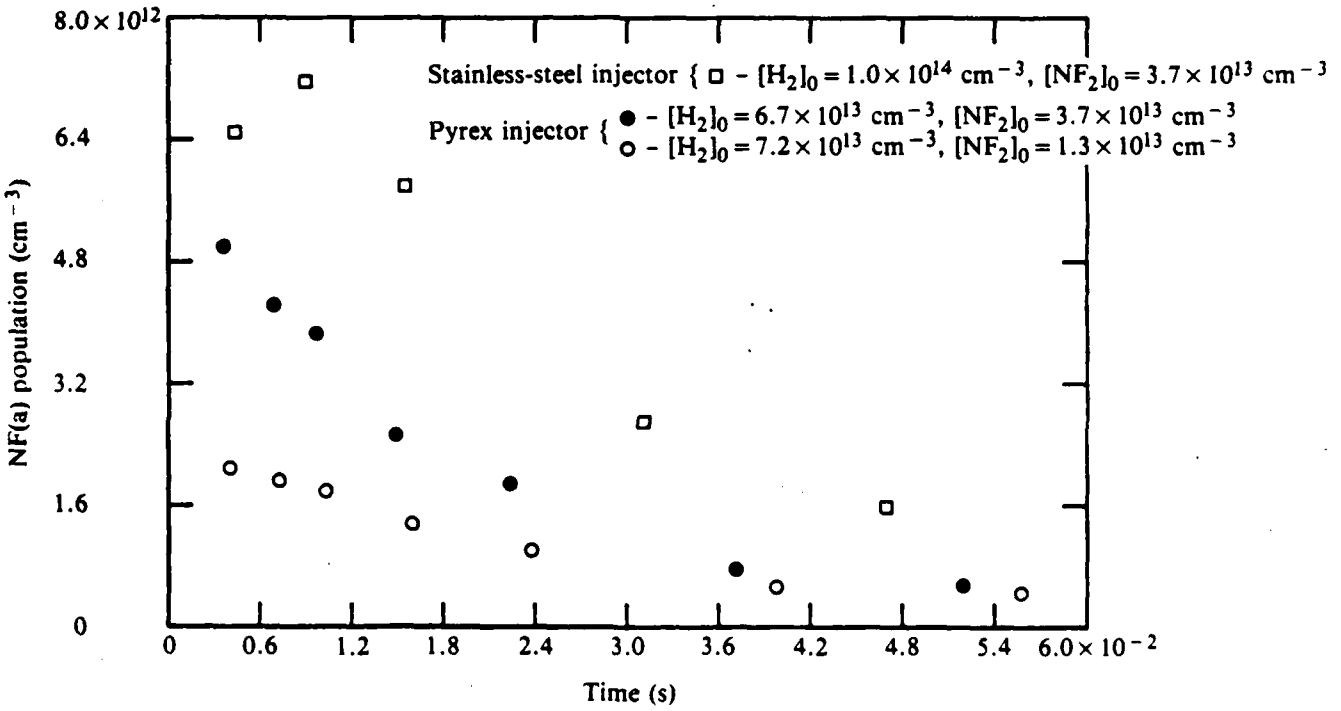

Figure 3. NF(a) population profiles from the H + NF_2 system.

resulting in a different $[N_2F_4]_o$. Since the fast H + NF_2 reaction has a branching ratio to NF(a) of 0.9 (Refs. 1 and 3) and the N_2F_4 dissociation is virtually complete (see section V below), it would be expected that the ratio of the peak [NF(a)] to $2[N_2F_4]_o$ would be near 1. However, ratios of 0.16 for $[N_2F_4]_o = 6.6 \times 10^{12}$ cm^{-3} and of 0.14 for $[N_2F_4]_o = 1.8 \times 10^{13}$ cm^{-3} were found. To ensure that reactions of NF_2 or N_2F_4 with the walls of the Pyrex injector were not causing the reduced NF(a) yields, a stainless steel injector was used to obtain a profile. In this case the peak [NF(a)] to $[N_2F_4]_o$ was still only 0.19. The delay in the NF(a) peak for the stainless steel injector was probably caused by an injector design with less efficient mixing than the Pyrex injector.

Since the efficient generation of electronically excited N_2 is predicated on the efficient production of NF(a), it is important to understand the apparently low NF(a) yields. At this time there is no definite answer, but some explanations should be considered. Equation (9) shows that uncertainties in the radiative rates for both the NF(a→X) transition and the O + NO emission cause corresponding uncertainties in the [NF(a)]s. Malins and Setser state that the uncertainty in their reported NF(a) radiative lifetime, caused by scatter in the data points, is ±10%, but that systematic errors are probably much larger (Ref. 3). In addition, the values used to obtain the average k_r used in the analysis ranged from 6 to 13 x 10^{-20} cm^3 s^{-1} mm^{-1}. Clearly, these are large sources of uncertainty in our NF(a) population measurements.

Another possible cause of low NF(a) yields is the loss of NF_2 resulting from disproportionation in the heated injector. The result (that the yields of Pyrex and stainless steel injectors are similar) indicates that direct reaction with the walls is not a problem. However, related Independent Research and Development (IRAD) studies at MDRL (Ref. 21) have shown that under suitable conditions the H + NF_2 flame can be initiated by the addition of undissociated H_2 to the output of heated Pyrex or stainless steel N_2F_4 injectors. Such a result indicates that the NF_2 in the injector is disproportionating to yield more reactive species such as F atoms. The degree of disproportionation has yet to be quantified.

There are two other possibilities that should be mentioned. One is that the branching ratio for the H + NF_2 reaction to form NF(a) may be less than the 0.9 reported in Reference 3. Given the importance of the branching ratio an independent measurement verifying the results of Reference 3 would be

useful. The final possibility to be considered is that there is an (as yet unidentified) fast NF(a) loss channel. The long decay-times observed for the NF(a) (Fig. 3) present an argument against such a rapid loss. However, a rapid equilibration between NF(a) and a more slowly quenched species could decrease the instantaneous NF(a) population while increasing the apparent NF(a) decay time.

b. $N_2(B)$ vibrational distribution--These measurements were performed in two parts. First, several spectra of the visible $N_2(B \rightarrow A)$ $\Delta v = 4$, 3, and 2 emission were analyzed to establish the $v = 2 \rightarrow v = 12$ relative vibrational distribution resulting from the $H + NF_2$ flame. Subsequent to these measurements, the relative populations in $v = 0 \rightarrow v = 5$ were obtained by analysis of a spectrum of the $\Delta v = 1$, 0, and -1 emission bands in the 850- to 1250-nm region. Table 2 gives the transitions and radiative rate constants used in the analysis of both these spectral regions. The two relative population distributions were linked by the procedure which follows.

The relative distribution determined from the visible spectra for $v = 2 \rightarrow v = 12$ is given in Table 3. It represents the average of six different scans of the $B \rightarrow A$ emission. The distribution determined from a particular spectrum was normalized to give $N_4 = 1.0$. The final relative population for a particular v was obtained by averaging over all the transitions in all the spectra that gave the relative population. For example, the relative population in $v = 6$ was obtained by averaging 18 values, three from each of the six spectra (Table 2). Five of the scans were performed with the 0.25-m monochromator and the same reagent flow conditions but with the NF_2 injector at different positions. For these spectra the substructure of the individual $v' \rightarrow v''$ transitions was not resolved and the required areas were determined from the peak heights and overall bandwidths. One spectrum was recorded with the 0.5-m monochromator. In this case the area of P_{11} branch of a given $v' - v''$ band was used to determine relative populations.

A single spectrum of the 850- to 1250-nm spectral region (Fig. 4) was used to determine the $v = 0 \rightarrow v = 5$ relative distribution. The results, again normalized to 1.0 at $v = 4$, are given in Table 3. The primary purpose of these measurements was to determine the relative population in $v = 0$ and $v = 1$. Normalization to 1.0 at $v = 4$ is useful for a convenient comparison, but does not necessarily give the best estimate of the $v = 0$ and $v = 1$

TABLE 2. $N_2(B-A)$ TRANSITIONS USED TO DETERMINE RELATIVE VIBRATIONAL POPULATIONS

v'	v''	λ (nm)	$A_{v'v''}$ ($10^4 s^{-1}$)
12	8	574	6.49
11	7	579	6.11
10	6	584	5.38
9	5	589	4.38
8	4	595	3.25
7	3	600	2.14
6	2	606	1.19
11	8	624	4.14
10	7	631	5.86
9	6	638	7.31
8	5	645	8.15
7	4	653	8.10
6	3	661	7.09
5	2	669	5.26
7	5	715	2.03
6	4	726	4.38
5	3	737	6.86
4	2	748	8.36
3	1	761	7.73
2	0	773	4.44
1	0	888	8.72
5	5	917	1.91
4	4	940	2.94
3	3	965	2.85
2	2	991	1.25
0	0	1047	6.25
1	2	1189	1.85
0	1	1232	3.56

relative populations. The v = 2 → v = 12 distribution from the visible emission was obtained from several measurements under a variety of experimental conditions and with two different optical detection systems. Clearly, it is the more precisely determined of the two. Thus, the best approach for linking the distributions is to fix the v = 2 → v = 12 distribution and normalize the v = 0 → v = 5 distribution to best fit the common v = 2 through v = 5 levels. The normalization factor C is obtained from the least-squares criterion

TABLE 3. RELATIVE $N_2(B)$ POPULATIONS FROM VISIBLE AND IR EMISSION BANDS[a]

Vibrational level	0	1	2	3	4	5	6	7	8	9	10	11	12
Relative population from IR bands[b]	2.02	1.37	1.46	0.86	1.00	1.59	—	—	—	—	—	—	—
Relative population from visible bands[c]	—	—	1.48 ±0.11	0.76 ±0.10	1.00 —	1.25 ±0.17	1.57 ±0.27	1.26 ±0.17	0.82 ±0.11	0.65 ±0.08	0.60 ±0.05	0.57 ±0.05	0.43 ±0.04

[a]Normalized to 1.00 at v = 4

[b]These relative populations were determined from one spectrum, hence no statistical analysis was done.

[c]Uncertainties represent one standard deviation of a single measurement from the mean.

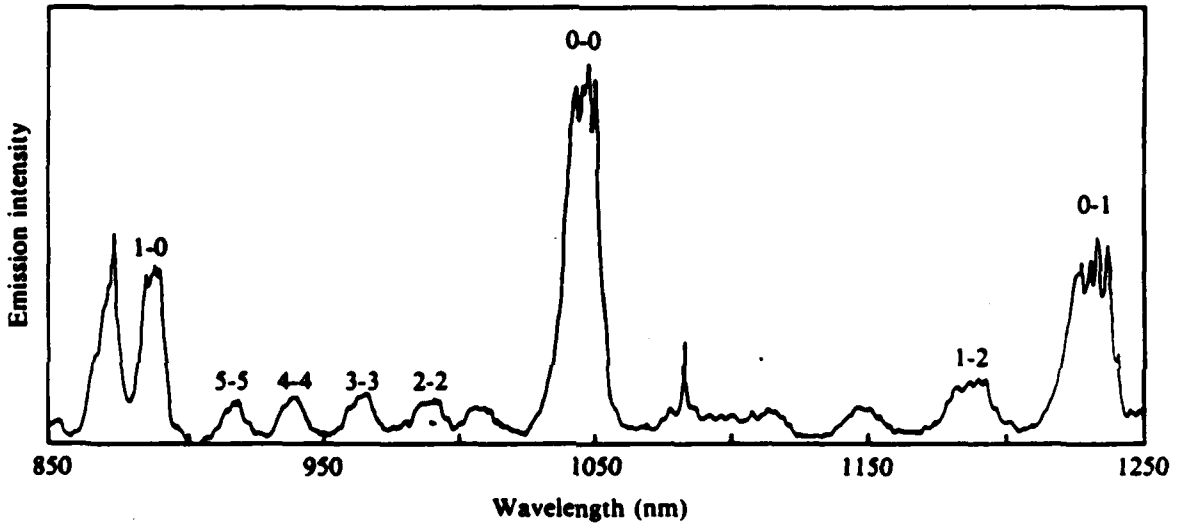

Figure 4. Near-IR emission spectrum of the H + NF_2 system.

$$\frac{\partial}{\partial C}\left(\sum_{v=2}^{5}(R_v - CR'_v)^2\right) = 0 \qquad (26)$$

where R_v is the relative population from the visible emission lines and R'_v that from the IR emission lines. The data in Table 3 provide a C value of 0.91. This value gives 1.85 and 1.26 as the best relative populations for v = 0 and v = 1, respectively. Figure 5 shows our best estimate of the overall $N_2(B)$ vibrational distribution.

The distribution shown in Figure 5 is somewhat different from that reported by previous investigators (Ref. 4) of the H + NF_2 flame. They find a

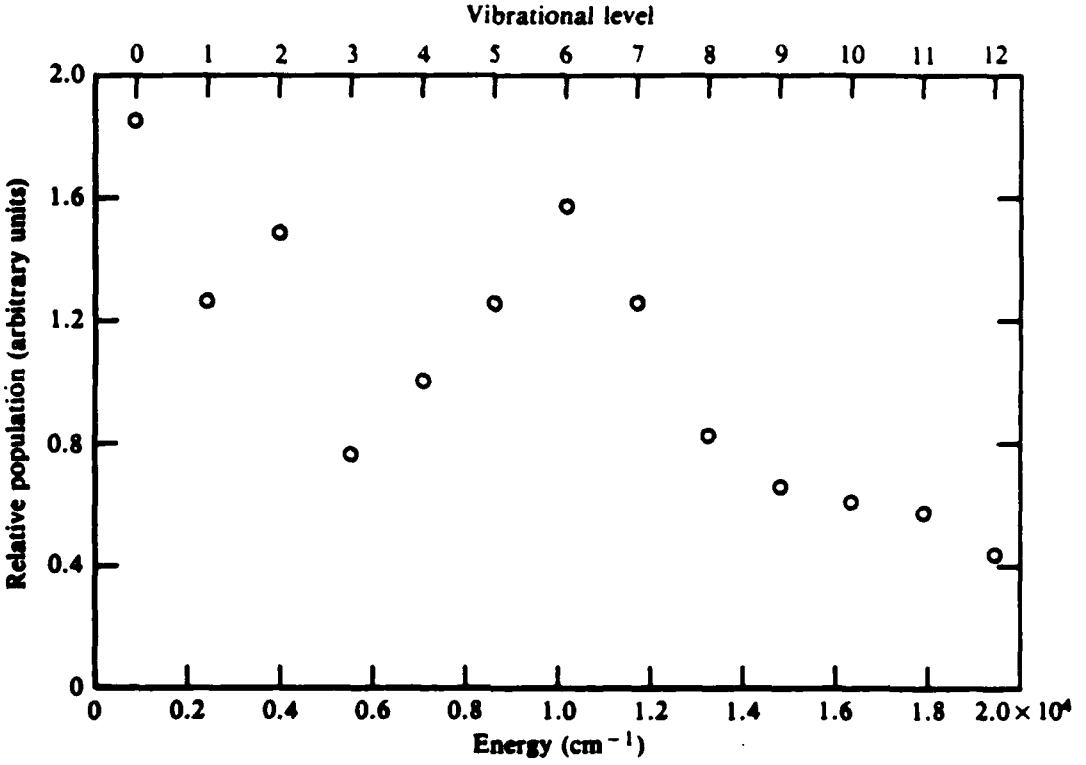

Figure 5. Relative vibrational distribution of $N_2(B)$ produced from $H + NF_2$.

monotonic fall in N_v with increasing v that could be fit to an apparent Boltzmann vibrational temperature of 8200 K. The distribution shown in Figure 5 can be explained by an examination of the kinetics of the collisional coupling of the A, B, and W states of N_2. A number of investigators have observed that $N_2(B)$ is efficiently coupled to the W state even by collisions with inert gases (Refs. 22-24). The v = 0 level of the W state is only 74 cm^{-1} higher in energy than v = 0 of the B state and the fundamental vibrational frequencies of the W and B are 1501 cm^{-1} and 1733 cm^{-1}, respectively. As a result, the B-W mixing might be expected to vary as a function of v due to changing energy-level mismatches up the vibrational manifold. Indeed, this has been reported by Rotem et al. (Ref. 22). They laser-excite the v = 5 and v = 6 levels of $N_2(B)$ in 270 Pa of Ar and observe the time evolution of the v = 2, 3, and 4 levels. At all delay times longer than a few microseconds they find that the population in v = 2 and v = 4 is larger than that in v = 3, exactly the effect demonstrated in Figure 5. Further evidence that the distribution shown in Figure 5 is correct is found in the results shown in Reference 25. The vibrational distribution of $N_2(B)$

formed from a dc discharge in a mixture of 130 Pa of N_2 and 2100 Pa of Ar was measured. The v=0 → v=4 portion of their measured distribution is remarkably similar to that reported here. This is to be expected if collisional coupling is important in determining the observed distribution. The populations in v = 5, 6, and 7 in Figure 5 are higher than those reported in Reference 25. This could be due to different coupling of the higher vibrational levels by the nitrogen in their system or because additional electronic states, such as the B' state, are produced in the chemical system; these electronic states could then couple to the B state. Such collisional coupling of the B and B' states has been reported (Ref. 26).

c. $N_2(B)$ population profiles and efficiencies--Using the procedure given in paragraph 2.c and the vibrational distribution from paragraph 4.b, $N_2(B)$ populations were determined as a function of injector position (i.e., time) for a variety of conditions. Six different profiles were measured with the Pyrex injector. Figure 6 shows the results from two experiments in which only the H_2 flows into the microwave discharge were varied. Two profiles obtained

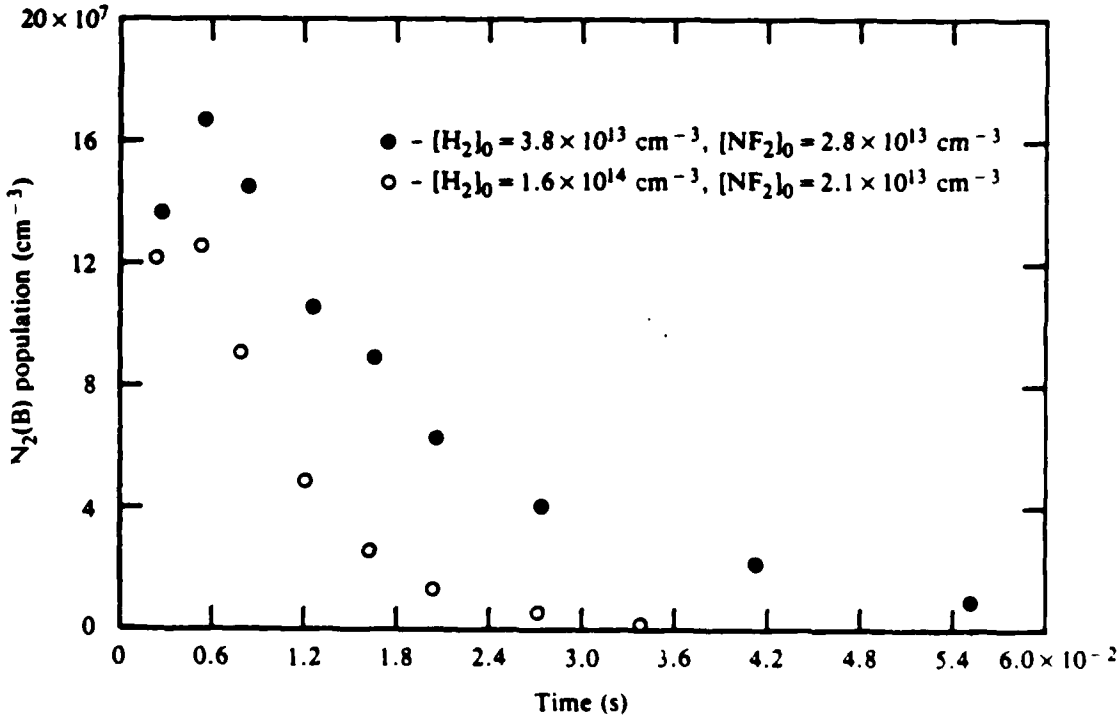

Figure 6. $N_2(B)$ population profiles using a microwave discharge in H_2/He as the H-atom source.

with F + D_2 as the D-atom source were also measured; the results are presented in Figure 7. In this case the conditions in the D-atom source were held constant and only the flows of the N_2F_4/He mixtures were varied. It should be noted that for these two measurements alone the usual halocarbon wax coating was replaced by a spray-on Teflon coating. Two final profiles obtained with the Pyrex injector and the microwave discharge source of H atoms are shown in Figure 8. In this case the discharge conditions were held constant and the N_2F_4/He flow through the injector was varied. Some heating of the gas near the injector occurred in all of these runs. Figure 9 shows a typical gas temperature (0.05 m below the observation ports) as a function of injector position profile.

As mentioned in the NF(a) profile section (paragraph 4.a), a measurement with a stainless steel injector was made to ascertain that wall reactions were not influencing the populations. The results for $N_2(B)$ are in Figure 10. A comparison with the results using the Pyrex injector reveal no significant difference.

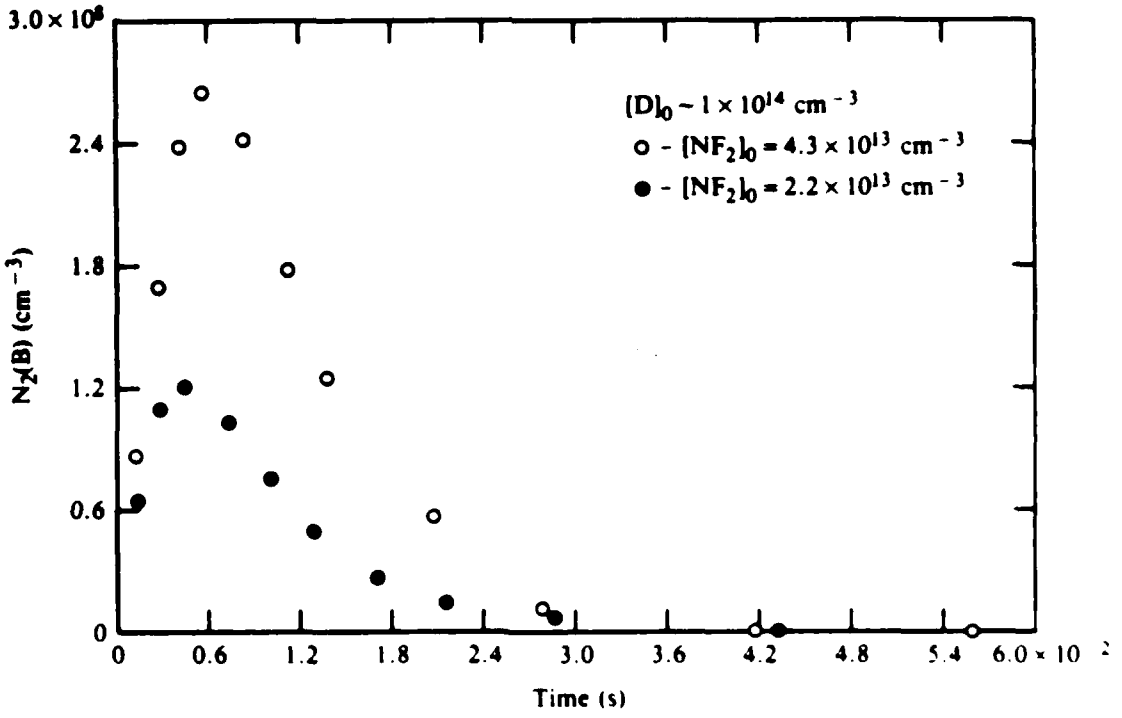

Figure 7. $N_2(B)$ population profiles using F + D_2 as the D-atom source.

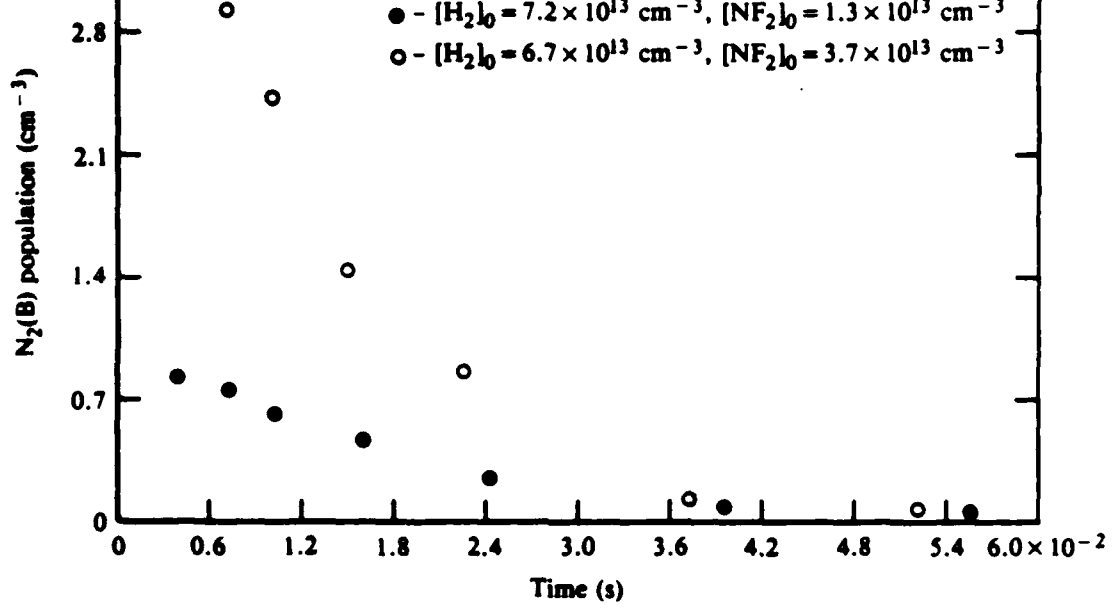

Figure 8. $N_2(B)$ population profiles using a microwave discharge in H_2/He as the H-atom source.

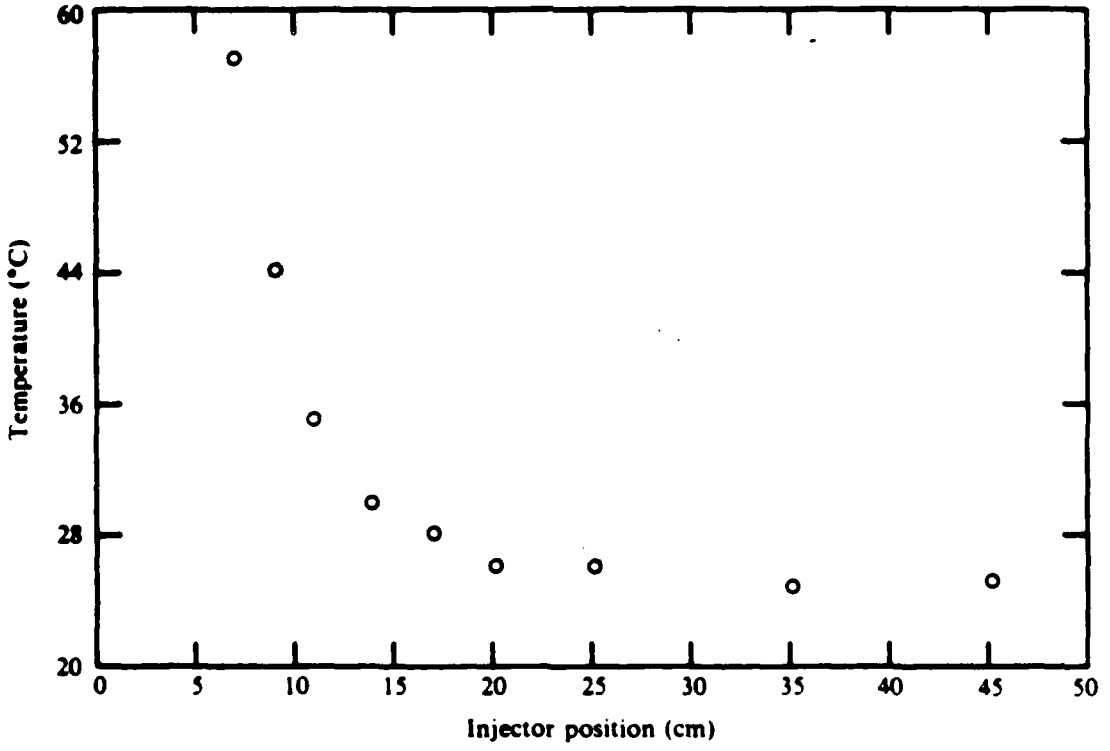

Figure 9. Typical temperature profile from the $H + NF_2$ measurements.

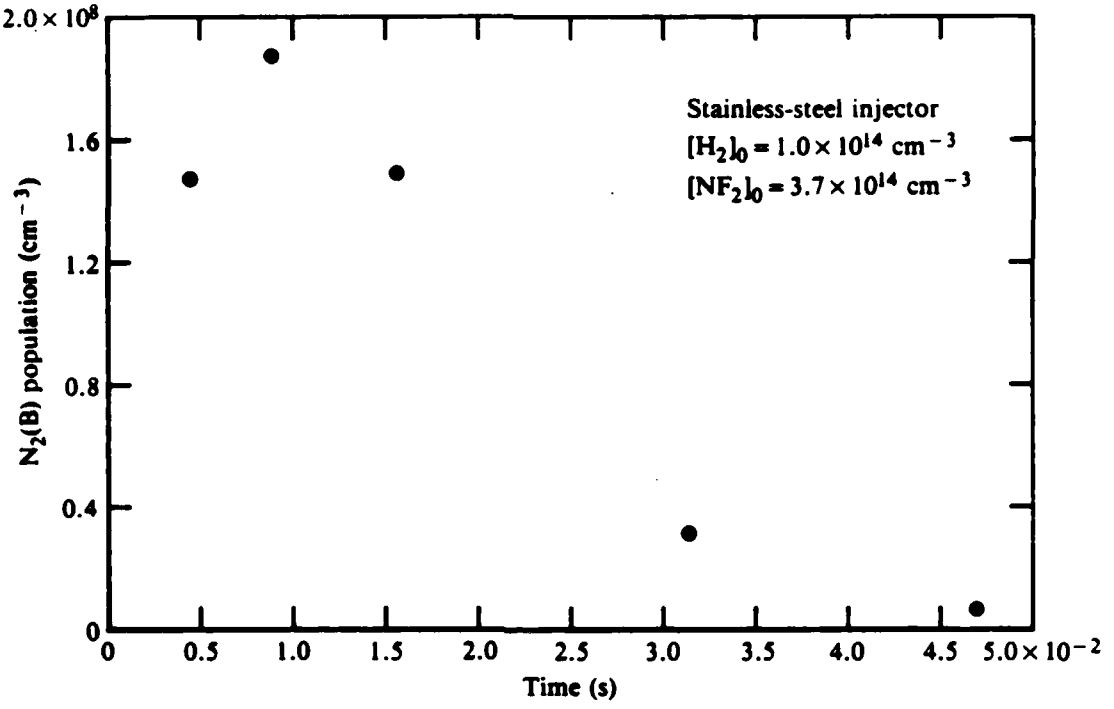

Figure 10. $N_2(B)$ population profiles using stainless-steel N_2F_4 injector.

From the profiles of $[N_2(B)]$ as a function of time, shown in Figures 6, 7, 9, and 10, the efficiency of $N_2(B)$ production can be determined as described in paragraph 2.b. The effective radiative lifetime of the $N_2(B)$ manifold was calculated to be 6.02 μs. The results are summarized in Table 4. In general, they are low and show no obvious trends relative to experimental condition or H(D) atom source. For the experiments in which both NF(a) and $N_2(B)$ were measured, an efficiency relative to the peak [NF(a)] was also calculated and is seen to be significantly higher. This further emphasizes the need to determine the reason for our apparently low NF(a) yields reported in paragraph 4.a.

d. NF(b) Population profiles--During the experiments to obtain the $N_2(B)$ profiles, shown in Figures 8 and 9, data were also obtained to allow determination of [NF(b)]s as outlined in paragraph 2.f. The results presented in Figures 11 and 12 show that the NF(b) profiles closely follow the $N_2(B)$ profiles. By noting that the NF(a) profiles in Figure 3 and the NF(b) profiles in Figure 12 were taken in the same experiments, and that the peak [NF(a)] to peak [NF(b)] ratio is >400 in both experiments, an interesting conclusion can

be made: excitation of NF(a) to NF(b) does not represent a significant loss channel for NF(a) under the conditions of these measurements.

TABLE 4. $N_2(B)$ PRODUCTION EFFICIENCIES

$[N_2F_4]_0$ (10^{13} cm^{-3})	Peak [NF(a)] (cm^{-3})	$N_2(B)$ Efficiency Relative to $[N_2F_4]_0$[c]	$N_2(B)$ Efficiency Relative to peak [NF(a)][d]
[a]1.4	—	0.044	—
[a]1.0	—	0.025	—
[b]1.1	—	0.023	—
[b]2.2	—	0.028	—
[a]0.66	2.1×10^{12}	0.036	0.23
[a]1.8	5.0×10^{12}	0.044	0.33
[a]1.8	7.2×10^{12}	0.0343	0.18

H(D) atom source:
[a]Microwave discharge in H_2/He
[b]$F + D_2$
[c]Efficiency = (total $N_2(B)$ produced/$[N_2F_4]_0$)
[d]Efficiency = 2(total $N_2(B)$ produced/peak [NF(a)])

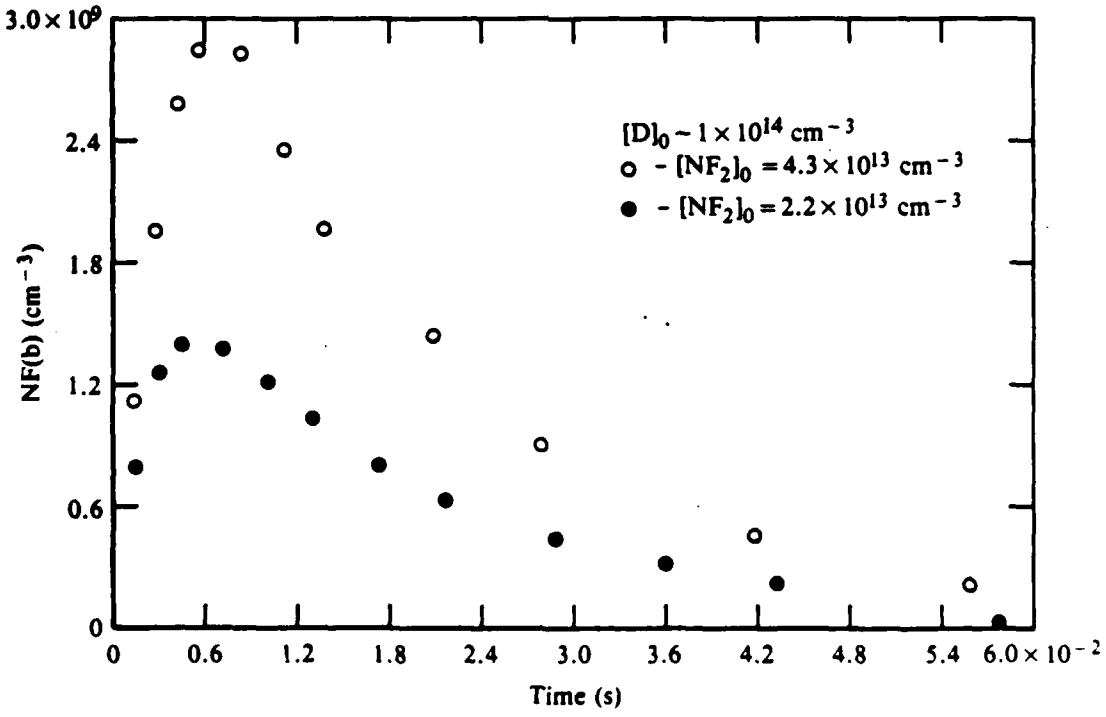

Figure 11. NF(b) population profiles using $F + D_2$ as the D-atom source.

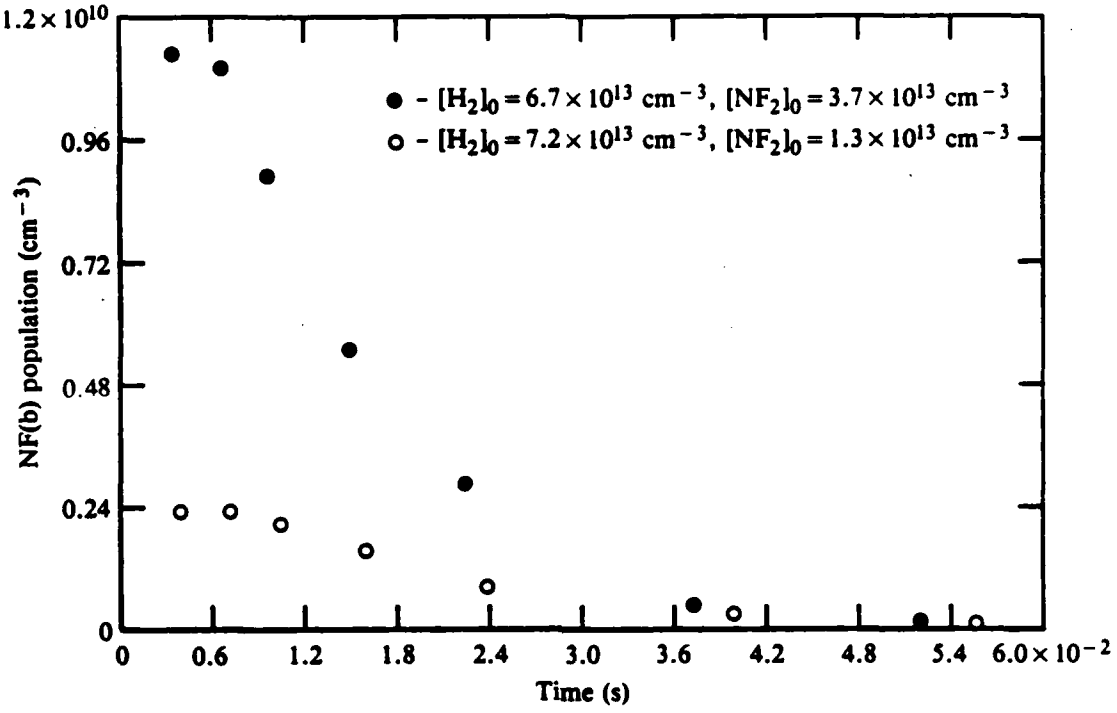

Figure 12. NF(b) population profiles using a microwave discharge in H_2/He as the H-atom source.

e. $N_2(A)$ population measurements--These measurements first required the determination of the relative spectral sensitivity of the diode-array detection system. Measurements were made at 280, 350, 436, and 546 nm as described in paragraphs 2.d and 3.b. The results are shown in Figure 13.

To test the $N_2(A)$ concentration measurement procedure and to obtain an estimate of $N_2(A)$ production in the H + NF_2 flame, four spectra were recorded in which the reference source of $N_2(A)$ was added to the usual flame. The experimental details are given in paragraph 3.b. The conditions for the spectra (Fig. 14) are given as follows.

Spectrum 1: Microwave discharge on, No H_2 (or H atoms), dc discharge (and $N_2(A)$) on, no N_2F_4.

Spectrum 2: Same as 1 except with cold N_2F_4 added (no NF_2).

Spectrum 3: Same as 2 except with H_2 (and thus H atoms) on and N_2F_4 heated to initiate the H + NF_2 system.

Spectrum 4: Same as 3 except dc discharge off.

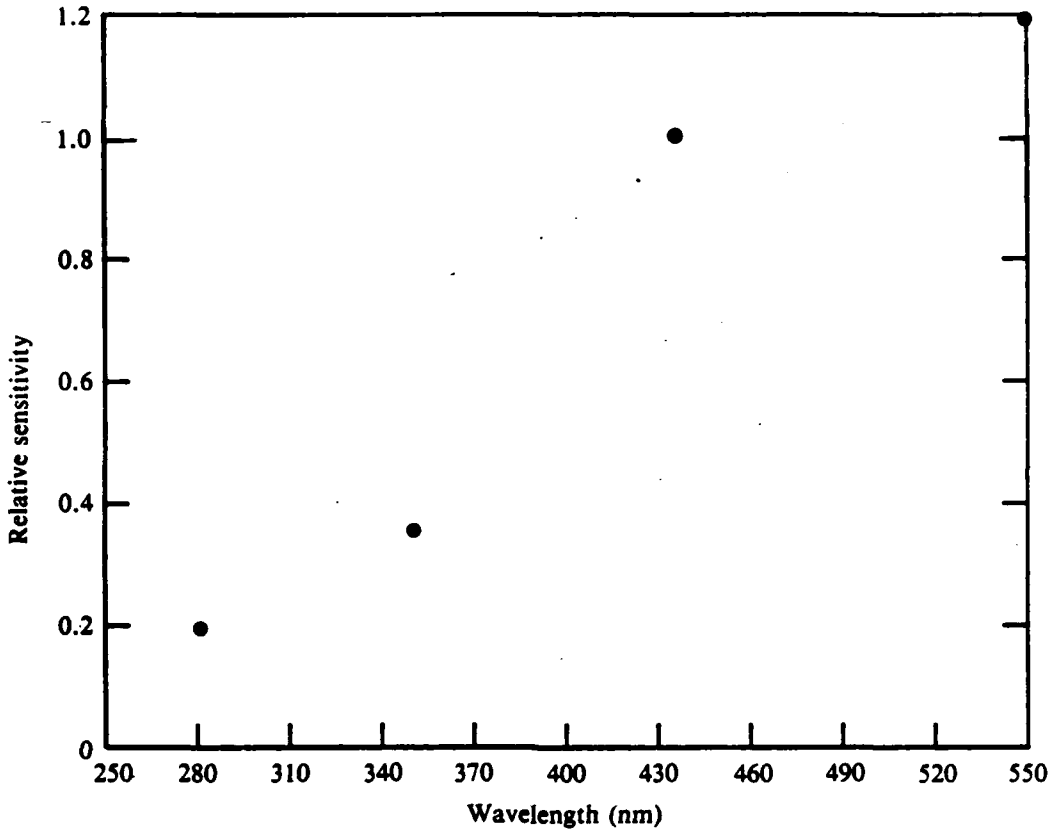

Figure 13. Relative photon sensitivity of the intensified diode-array detection system normalized to 1 at 546 nm.

Before performing a quantitative $N_2(A)$ analysis, it is appropriate to make some qualitative observations concerning the spectra in Figure 14. The $N_2(A-X)$ $v'= 0 \rightarrow v''= 6$ line at 276 nm is strongest in spectrum 1, where only the dc discharge source for $N_2(A)$ and the microwave discharge in He are on. There are weak NO lines in spectrum 1 due to NO generated in the He microwave discharge and subsequently excited by energy transfer from $N_2(A)$. This mode of NO generation was verified by the disappearance of the NO lines when the microwave discharge was turned off (not shown in Figure 14). When cold N_2F_4 was added (spectrum 2), the NO emission lines increased in intensity and the $N_2(A)$ emission became somewhat quenched. This change indicates that NO must be contaminating the N_2F_4. When the N_2F_4 was heated to generate NF_2 and H_2 was added to the microwave discharge to generate H atoms, emission from the H + NF_2 flame resulted (spectrum 3). Spectrum 3 displays a dramatic increase in the NO emission lines, but the $N_2(A)$ emission lines are, at best, comparable

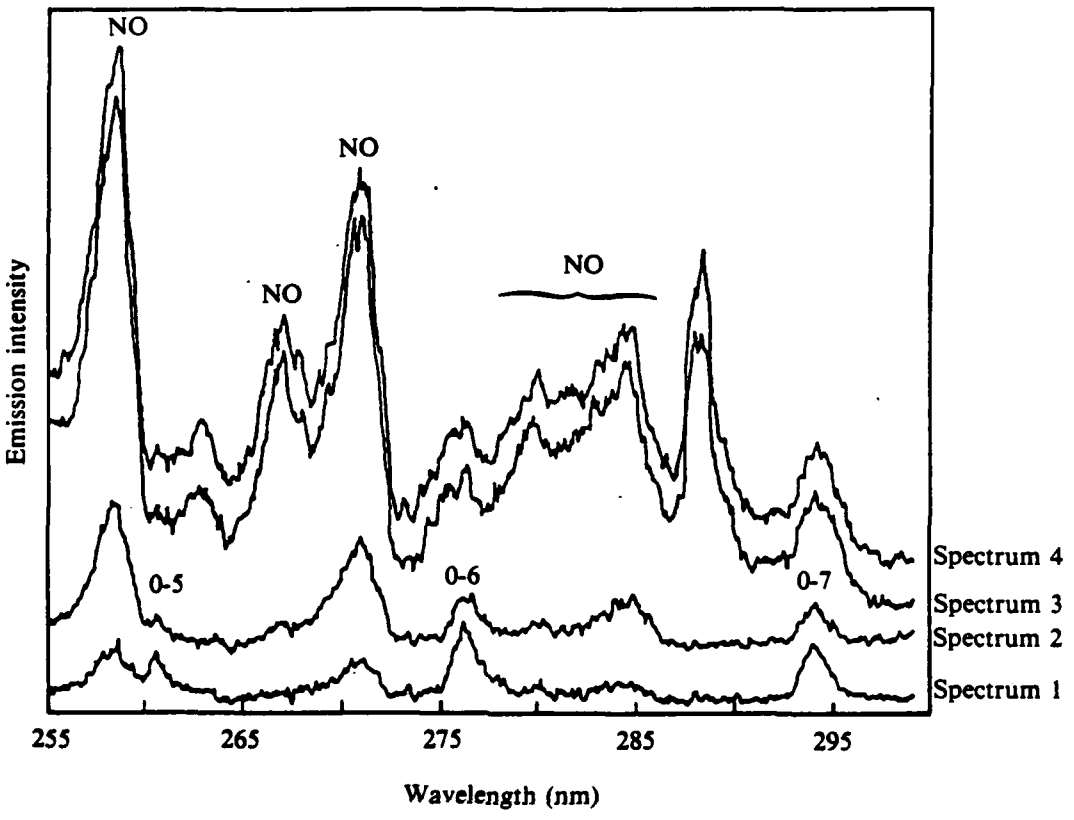

Figure 14. $N_2(A)$ spectra with and without the $H + NF_2$ system. Spectra origins are offset for clarity (see text for parameter details).

to those in spectrum 1. Turning off the dc discharge $N_2(A)$ source has a negligible effect (spectrum 4). The fact that there is no $N_2(A)$ concentration buildup when the $H + NF_2$ system is initiated implies that an $N_2(A)$ loss channel must exist which is significantly greater than the wall loss rate.

Spectrum 1 of Figure 14 provides an upper limit for the $N_2(A)$ concentration. The calibration factor needed to convert the integrated $N_2(A\text{-}X,0\text{-}6)$ line to concentration was calculated as described earlier in paragraph 2.4. Use of the $N_2(A,v=0)$ radiative lifetime of 1.9 s (Ref. 7), a Franck-Condon factor for the 0-6 component of 0.191 (Ref. 7), plus the assumption that there is no variation of the electronic transition moment with R-centroid, establishes the $N_2(A\text{-}X,0\text{-}6)$ radiative rate as 0.101 s^{-1}. The resulting calibration factor applied to the integrated 0-6 line in spectrum 1 yields $[N_2(A,v=0)] \sim 2 \times 10^9$ cm^{-3}.

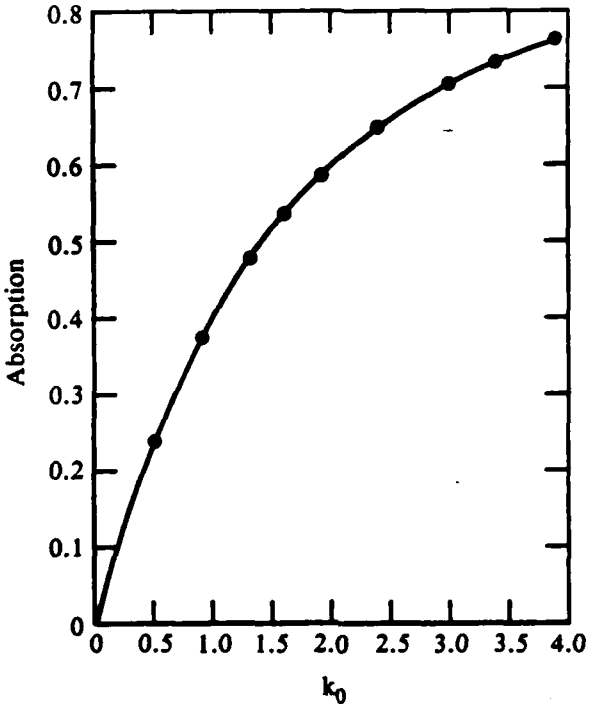

Figure 15. Curve of growth for $\alpha = \sqrt{2}$.

To estimate the $N_2(A)$ concentration under typical flame conditions, spectra in the 250- to 300-nm region were recorded along with the NF(a), NF(b), and $N_2(B)$ data used for Figures 3, 8, and 12. Because the slit width for these spectra was 25 μm instead of the 100 μm used for the $N_2(A)$ measurements, it was necessary to redetermine the calibration factor needed to extract $N_2(A,v=0)$ concentrations. Because of the smaller slit widths, the signal-to-noise was less than that of the spectra shown in Figure 14. Therefore, it was only possible to place upper limits on the $N_2(A,v=0)$ concentrations of $\sim 8 \times 10^8$ cm^{-3} for $[N_2F_4]_o = 6.6 \times 10^{12}$ cm^{-3} and $\sim 3 \times 10^9$ cm^{-3} for $[N_2F_4]_o = 1.8 \times 10^{13}$ cm^{-3}.

Since $N_2(A,v=0)$ is only part of the total $N_2(A)$ created by radiative cascading from $N_2(B)$, the $N_2(A)$ and $N_2(B)$ concentrations are consistent with a model in which $N_2(A)$ is produced by radiative decay of $N_2(B)$ and lost by processes significantly faster than wall quenching. A measurement of the rate constant for $N_2(A)$ quenching by H atoms, described in Section IV.3, leads us to propose that this quenching is that fast loss process.

IV. KINETICS

1. RATE CONSTANTS FOR THE REACTIONS OF $N(^2D)$ ATOMS WITH O_2, H_2 AND HF

a. Introduction--Hydrogen fluoride (HF) is a high-concentration byproduct of the H + NF_2 flame chemistry. When H_2 is used as the source of H atoms in the H + NF_2 flame to generate $N_2(A)$, H_2 is found to be a high-concentration constituent of the flame reaction mixture. Both HF and H_2 will compete with $NF(a^1\Delta)$, via reactions (27) and (28), for the $N(^2D)$ atoms produced by the flame chemistry.

$$N(^2D) + H_2 \rightarrow N(^4S) + H_2$$

$$\rightarrow NH(X) + H \qquad (27)$$

$$N(^2D) + HF \rightarrow N(^4S) + HF \qquad (28)$$

The extent to which this competition for $N(^2D)$ atoms affects the efficiency of $N_2(A)$ production in the H + NF_2 flame will depend mainly on the relative concentrations of H_2 and HF in the flame reaction mixture and the magnitudes of the rate constants for reactions (27) and (28).

Descriptions follow of the experiments performed to measure the rate constants for removal of $N(^2D)$ atoms by O_2, HF, and H_2. The rate constant for the $N(^2D)$ + O_2 reaction has been measured by several other workers (Table 5) and serves as a suitable reference reaction to test the experiment for systematic errors. The rate constant for the $N(^2D)$ + H_2 reaction has also been measured previously but not as extensively as that for the O_2 reaction and has only been measured once before in a discharge-flow experiment in which EPR was used to monitor the $N(^2D)$ atoms (Table 7). To the best of our knowledge, the rate constant for the removal of $N(^2D)$ by HF has not been measured previously.

b. Theory--The relationship between the absorber concentration [N], oscillator strength (f), and the integral of the absorption coefficient (k_ν) at frequency (ν) in Equation (29), can be used with the relationship relating fractional absorption A to k_ν, Equation (30), to calculate absorber

concentrations from simple fractional-absorption measurements made in a resonance absorption experiment

$$[N] = (mc/\pi e^2 f) \int_{-\infty}^{\infty} k_\nu \, d\nu \tag{29}$$

$$A = (I_o - I_{trans})/I_o =$$

$$\{\int_{-\infty}^{\infty} I(\nu) \, [1 - e^{(-k\nu\ell)}] \, d\nu\}/\int_{-\infty}^{\infty} I(\nu) \, d\nu \tag{30}$$

The precise analysis to determine [N] from measurements of A using Equations (29) and (30) has been presented elsewhere (Refs. 27-29). The relevant factors in this analysis are the line profiles of source and absorber species (Ref. 30). The absorber line-shape follows a Voigt profile (Ref. 27) which is the convolution of a Gaussian function from the Doppler width with a Lorentzian function from the pressure-broadened line width. In atomic resonance studies at low pressures (< 0.65 kPa) the absorbers are in equilibrium with the carrier gas at 298 K and pressure broadening is slight or negligible (Refs. 27, 31, and 32). Thus, the absorber line-shape closely approximates a Doppler profile which is Gaussian. When a low-power-density microwave plasma is used as the source of resonance radiation and this radiation is non-reversed, a Doppler model for the source-line profile has also been shown to be applicable (Ref. 27-29, and 33) even though the effective temperature of the source radiation (T_s) is much greater than the typical temperature of absorbers (T_a) . Typically, T_a = 398 K.

The calculation of absorber concentration [N] is based on Equation (31), assuming Doppler line models:

$$k_o\ell = (2/\Delta\nu_D) \, (\ln 2/\pi)^{1/2} \, (\pi e^2/mc) \, [N] f \ell \tag{31}$$

where k_o is the absorption coefficient at the line center and hence $k_o\ell$ is the optical depth of the absorber. $\Delta\nu_D$ is the Doppler width and is defined by Equation (32):

$$\Delta\nu_D = (2/\lambda_o c) \, (2RT \ln 2/M)^{1/2} \, cm^{-1} \tag{32}$$

where M is the atomic mass and λ_o is the wavelength at the line center. The absorption coefficient k_o is related to k_ν through Equation (33):

$$k_\nu = k_o \exp\{-[2(\nu - \nu_o\sqrt{\ln 2}/\Delta\nu_D]^2\} \quad (33)$$

Computer programs have been developed to evaluate numerically the function relating $k_o\ell$ to A for any value of α [$\alpha = \sqrt{(T_s/T_a)}$] by use of Equations (30) and (33) (Refs. 30 and 33). This function is insensitive to small amounts of pressure broadening and is based on the assumption of a nonreversed source-line profile. Figure 15 is an example of the resulting curve of growth which relates $k_o\ell$ to A for $\alpha = \sqrt{2}$.

The theoretical analysis was developed for a single resonance line. In the experiments which follow, line absorptions were measured on an unresolved doublet. In this case an extension of the Doppler model analysis was used. The extension is simple since the component lines of the doublet have spacings which are large compared with their mean Doppler width at 298 K and, thus, there is no cross coupling between the two sets of emission and absorption lines for the doublet.

For the three lines of the $2^2D^o - 3^2P$ transition at 149.3 nm, the sum rules based on Russell-Saunders coupling (for light atoms) require the component line intensities to be in the ratio 9:1:5 and the peak absorption coefficients to be in the same ratio (Ref. 34). Thus, for the unresolved doublet, the intensities and absorption coefficients are in the ratio 9:1. The total absorption coefficient for the doublet (k_o) is the sum of its component line absorption coefficients ($k_o' + k_o''$) where k_o' is the absorption coefficient of the stronger line and k_o'' is the absorption coefficient of the weaker line. From the ratio of the absorption coefficients it can be seen that $k_o'' = k_o'/9$ and $k_o = 10\ k_o'/9$; thus, the absorption coefficient for the unresolved doublet can be expressed in terms of the absorption coefficient of one of its component lines. As such, this absorption coefficient can be used in Equation (31) with the mean oscillator strength for the unresolved multiplet to calculate the concentration of absorbers producing the fractional absorption recorded in the experiment. The mean oscillator strength of the unresolved doublet is calculated from

$$\bar{f} = \sum_L g_L f_{Lu} / \sum_L g_L \qquad (34)$$

where g_L is the statistical weight of the lower substate and f_{Lu} is the oscillator strength for the transition to that substate. The mean f-value for the N(^{2}D) doublet at 149.3 nm is 0.052 (Ref. 34). (The value of $k_o'\ell$ for a given fractional absorption, A, is determined as described above).

An equivalent, alternative approach can also be used to calculate the N(^{2}D) atom concentration from the absorption of the unresolved doublet via Equation (31). In this case the corresponding value of $k_o'\ell$ for a given absorption is used along with the oscillator strength of the stronger component line (f'_{LU} = 0.078). In this case, however, the calculated atom concentration is 0.6[N(^{2}D)] because of the 6:4 statistical weights of the J = 5/2 and 3/2 substates of the doublet at 149.3 nm.

c. Experiment--The discharge flow atomic resonance absorption apparatus is schematically represented in Figure 16. It consists of a flow tube with an absorption cell at a fixed observation point to which was connected a resonance lamp and a monochromator. The lamp is a 2.45-GHz microwave discharge in ultrahigh purity helium (Mattheson, 99.9999%) to which was added a trace of N_2 N_2 at a total pressure of 0.13 kPa. The monochromator (ARC VM502 V) has a 0.2-m focal length and contains an aberration-corrected 1200-line mm^{-1} concave holographic grating overcoated with magnesium fluoride (MgF_2). The monochromator provides an aperture ratio of f/4.5 and a linear dispersion of 4.0 nm mm^{-1} in the first order. The detector is a gallium arsenide photomultiplier (EMI 9558QB) with a sodium salicylate phosphor coated window mounted in a temperature controlled housing (Pacific Instruments). The MgF_2 windows at the fixed observation point isolate the flow tube gases from the monochromator and lamp. Figure 17 is a typical spectrum of the almost complete resolution of the N(^{2}D) apparent doublet at 149.3 nm [actually a triplet consisting of two close lines at 149.26 and 149.28 nm and one line at 149.47 nm]. The resolving power of the monochromator and radiation-detection system was not sufficient to resolve the 149.26- and 149.28-nm doublet.

The N(^{2}D) atoms were produced upstream in the flow tube by a 2.45 GHz microwave discharge in 0.4 kPa of high-purity Ar carrier gas (Matheson)

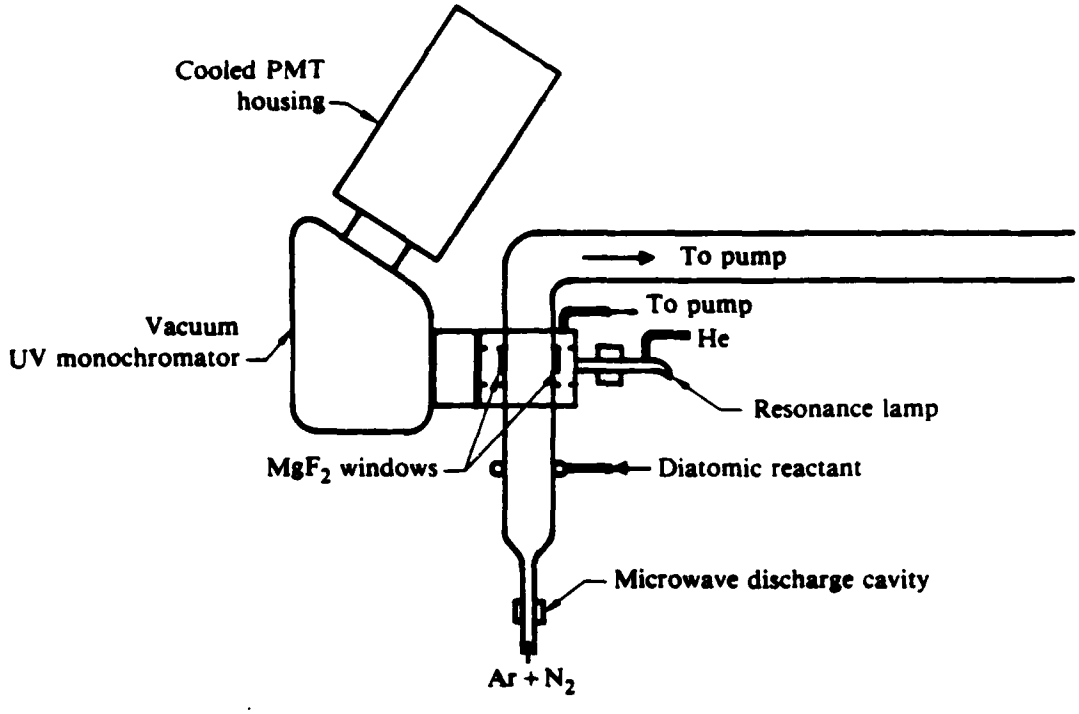

Figure 16. Schematic of discharge flow atomic-resonance absorption apparatus.

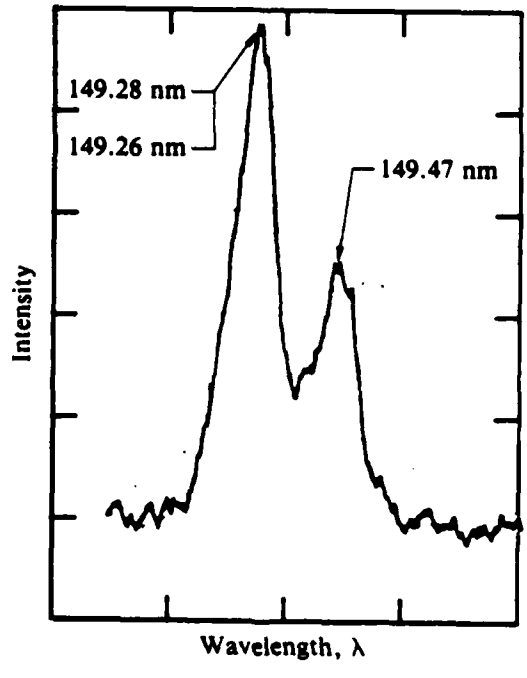

Figure 17. The N(^{2}D) apparent doublet at 149.3 nm.

containing a small, known amount of added N_2 (usually 2%). Loss of $N(^2D)$ atoms by wall deactivation is essentially inversely proportional to the total flow-tube pressure; therefore, a high total pressure had to be maintained in the flow tube to obtain a measurable concentration of $N(^2D)$ atoms at the fixed observation point. Also, following the recommendation of Fell et al. (Ref. 35), the $N(^2D)$ atom discharge was situated ~0.2 m upstream of the reactant injector. At shorter distances between discharge and injector, substantially larger rate constants had been measured by Fell and coworkers. They attributed this effect to the fragmentation of reactant molecules by energetic discharge byproducts which appeared to survive up to at least 0.13 m downstream of the discharge. The diatomic reactants O_2, H_2 (Union Carbide) and HF (Matheson) were injected into the flow tube separately through an externally mounted ring injector. The ring injector was used to assist the rapid mixing of reagents without obstructing the flow. The diatomic reactants were prediluted in carrier gas such that the addition of this mixture contributed less than 10% of the total carrier gas flow but provided reactant concentrations in the 10^{13} - 10^{14} cm^{-3} range. The ring injector was situated 0.12 m upstream of the fixed observation point. The flow tube was throttled downstream of the fixed observation point to achieve reaction times on the order of 3×10^{-3} s between the injector and the fixed observation point.

d. Results--The rate constants were determined under pseudo-first-order kinetic conditions with the fixed observation point method. The first-order decay rate of a species measured at the fixed observation point is independent of concurrent first-order processes such as wall removal. Thus, a simple pseudo-first-order rate expression may be used to find the rate constant k (Ref. 36). For the general reaction

$$N(^2D) + X \rightarrow \text{Products} \tag{35}$$

where $[N(^2D)]_o \ll [X]$, the integrated rate equation becomes

$$\ln([N^2D)]_o/[N(^2D)]_t) = k[X]t \tag{36}$$

The reaction time, t, is calculated from the gas flow velocity $\bar{u}$, and the simple plug-flow model is assumed. This model assumes a constant flow

velocity across the tube, uniform and rapid mixing upon introduction of reactants into the carrier gas flow, and a constant concentration of reagents along the flow tube. The model neglects axial diffusion (Ref. 37-39). The plug-flow assumption is not totally valid under the typical experimental conditions. The gas flow is in transition between simple plug-flow and laminar flow, and as such, a parabolic velocity distribution exists across the flow tube. Under fully developed laminar flow conditions, the plug-flow rate constant would have to be multiplied by a correction factor of 1.62 (Refs. 40, 41). In the intermediate flow condition, a transition length can be calculated which characterizes the parabolic velocity-distribution region (Ref. 42). The transition length in these experiments is 0.5 m with Ar carrier gas as the major gas-mixture constituent. The reaction zone is, therefore, only one quarter of the transition length and, thus, the full correction factor of 1.62 is not valid either. The appropriate correction factor must lie between 1.0 and 1.62. In previous $N(^2D)$ atom kinetics studies, the procedure under such circumstances has been to assume a mean correction factor of 1.3 (Refs. 34, 35). The validity of this assumption has been verified (Ref. 43) and, hence, this correction factor has been used in the kinetic analysis. The error limits on the corrected rate constants have been suitably increased to account for the uncertainty introduced by use of an average correction factor.

(1) $N(^2D) + O_2$ (room temperature 298 K)--Oxygen flows giving concentrations in the range $8 \times 10^{12} < [O_2]_o < 1.3 \times 10^{14}$ cm^{-3} were introduced into the $N(^2D)$ atom flow at a fixed inlet jet that was a known distance from the resonance lamp axis; thus, for a given total pressure and sum of reagent flows, a reaction time t was fixed for a given experiment. Good linear plots of $\ln\{k_o\ell_{max}/k_o\ell_{O_2}\}$ ($k_o\ell \propto [N]$, Eq. 31) against $[O_2]$ were obtained with initial $[N(^2D)]$ of $\sim 1 \times 10^{12}$ cm^{-3}. A two-parameter least-squares analysis of these data provided slopes which, when divided by the reaction time t, yielded the uncorrected observed rate constant $k(\ell)$. The deviation from plug flow arising from the parabolic velocity distribution across the flow tube was accounted for by multiplying $k(\ell)$ by the correction factor of 1.3, yielding $k(\ell)$corr. Tables 5 and 6 present data from two independent sets of measurements of $k(\ell)$ yielding a mean value of $k(\ell)$corr of $(6.6 \pm 1.0) \times 10^{-12}$ cm^3 s^{-1}. Figure 18 is a plot of the data presented in Table 7. This measurement of $k(\ell)$corr is

presented in Table 7 with other published measurements of k(ℓ)corr, for comparison (Refs. 8, 10, 34, 35, 43-45,).

TABLE 5. KINETIC DATA FOR THE $N(^2D) + O_2$ STUDY (1)

(1) $[O_2]$ ($\times 10^{13}$ cm^{-3})	(2) $\ln\left(\frac{k_\phi \ell_{(max)}}{k_\phi \ell_{(O_2)}}\right)$	(3) k(1) ($\times 10^{-12}$ cm^3 s^{-1})
3.43	0.299	5.34
5.30	0.423	4.90
7.30	0.540	4.54
10.02	0.793	4.85
12.50	1.153	5.66
10.29	0.943	5.62
8.76	0.836	5.85
6.70	0.600	5.49
4.80	0.451	5.76
3.33	0.318	5.85
1.00	0.210	5.12

$\bar{u} = 7.18 \times 10^3$ cm s^{-1}, $t = 1.63 \times 10^{-3}$ s.

k(1) corr = $(6.6 \pm 0.8) \times 10^{-12}$ cm^3 s^{-1}.[a]

[a]This rate constant is the product of the correction factor of 1.3 and the slope of the unweighted least squares fit to the data in columns (1) and (2) above. The error reflects the statistical uncertainty (1σ) and the uncertainty introduced by using the mean correction factor.

TABLE 6. KINETIC DATA FOR THE $N(^2D) + O_2$ STUDY (2)

(1) $[O_2]$ ($\times 10^{13}$ cm^{-3})	(2) $\ln\left(\frac{k_\phi \ell_{(max)}}{k_\phi \ell_{(O_2)}}\right)$	(3) k(1) ($\times 10^{-12}$ cm^3 s^{-1})
2.20	0.359	5.26
4.75	0.674	4.58
8.14	1.331	5.27
4.13	0.792	6.18

$\bar{u} = 7.40 \times 10^3$ cm s^{-1}, $t = 3.1 \times 10^{-3}$ s.

k(1) corr = $(6.7 \pm 1.0) \times 10^{-12}$ cm^3 s^{-1}.[a]

[a]This rate constant is the product of the correction factor of 1.3 and the slope of the unweighted least squares fit to the data in columns (1) and (2) above. The error reflects the statistical uncertainty (1σ) and the uncertainty introduced by using the mean correction factor.

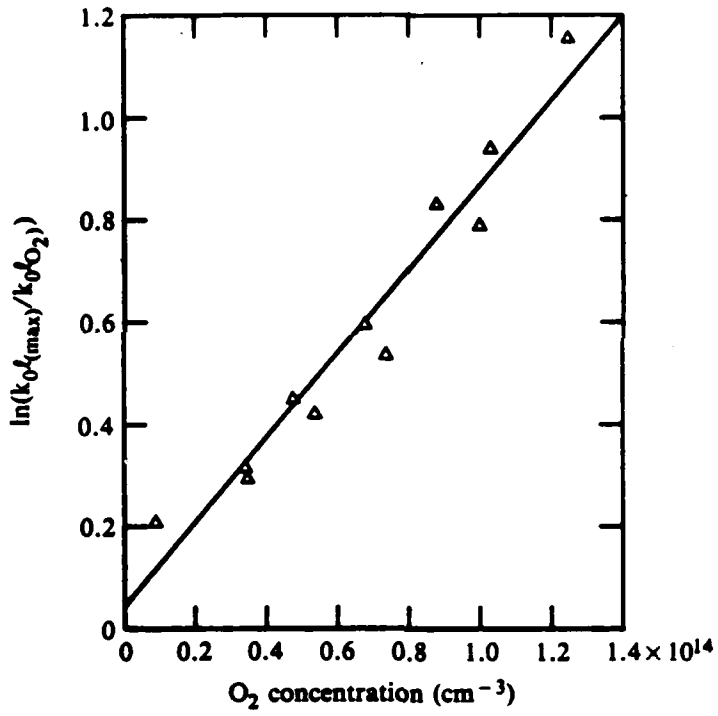

Figure 18. Typical pseudo-first-order kinetic data for the $N(^2D) + O_2$ study.

TABLE 7. MEASUREMENTS OF $k_{N(^2D)+O_2}$ AND $k_{N(^2D)+H_2}$

	k ($cm^3\ s^{-1}$)	Reference
$N(^2D) + O_2$	$(6.6 \pm 1.0) \times 10^{-12}$	this work
	7×10^{-12}	8
	$(6 \pm 2) \times 10^{-12}$	34
	7.4×10^{-12}	44
	$(5.2 \pm 0.4) \times 10^{-12}$	10
	$(5.8 \pm 0.5) \times 10^{-12}$	45
	$(5.49 \pm 0.3) \times 10^{-12}$	43
	6.1×10^{-12}	35
$N(^2D) + H_2$	$(1.8 \pm 0.8) \times 10^{-12}$	this work
	5×10^{-12}	8
	$(2.1 \pm 0.3) \times 10^{-12}$	10
	$(2.7 \pm 0.2) \times 10^{-12}$	46
	3.5×10^{-12}	35

(2) $N(^2D) + H_2$ (room temperature 298 K)--Hydrogen flows with concentrations in the range $5 \times 10^{13} < [H_2] < 3 \times 10^{14}$ cm^{-3} were introduced into the $N(^2D)$ atom flow at the fixed inlet jet (as for the O_2 experiments). For a given reaction time t, good linear plots of $\ln\{k_o \ell_{max} / k_o \ell_{H_2}\}$ against $[H_2]$ were obtained (Fig. 19), thus yielding the uncorrected observed rate constant k(2). Tables 8 and 9 present the data for two independent sets of measurements of k(2) yielding a mean value of k(2)corr of $(1.8 \pm 0.8) \times 10^{-12}$ cm^3 s^{-1}. This measurement of k(2)corr is presented in Table 7 with other published measurements of k(2)corr for comparison (Ref. 8, 10, 35, 46).

(3) $N(^2D)$ + HF (room temperature 298 K)--The HF flows with concentrations in the range $3 \times 10^{13} < [HF] < 7 \times 10^{14}$ cm^{-3} were introduced into the $N(^2D)$ atom flow at the fixed inlet jet. For a given reaction time t, good linear plots of $\ln\{k_o \ell_{max} / k_o \ell_{HF}\}$ against HF were obtained (Fig. 20), yielding an uncorrected rate constant k(3). Table 10 contains the data from three independent sets of measurements of k(3), yielding a mean value for k(3)corr of $(1.0 \pm 0.3) \times 10^{-12}$ cm^3 s^{-1}.

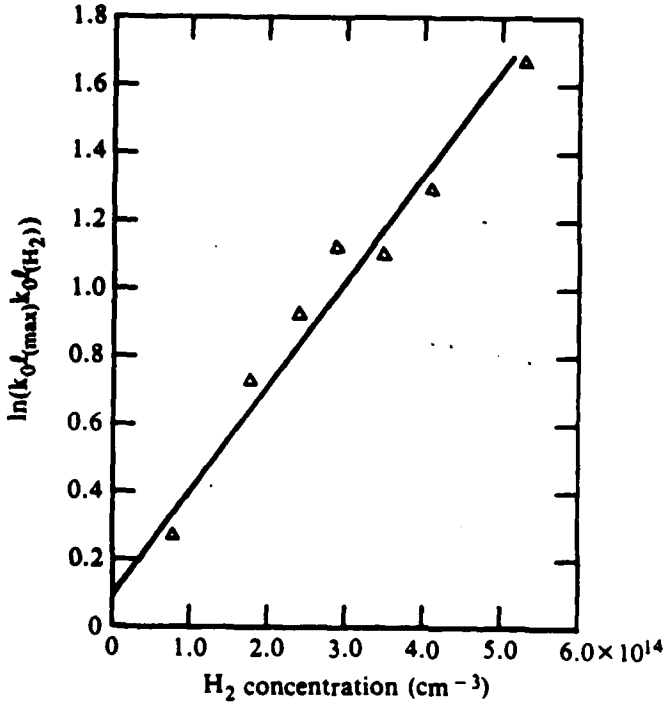

Figure 19. Typical pseudo-first-order kinetic data for the $N(^2D) + H_2$ study.

TABLE 8. KINETIC DATA FOR THE $N(^2D) + H_2$ STUDY (1)

(1) $[H_2]$ ($\times 10^{14}$ cm^{-3})	(2) $\ln\left(\frac{k_0 l_{(max)}}{k_0 l_{(H_2)}}\right)$	(3) k(2) ($\times 10^{-12}$ cm^3 s^{-1})
2.9	1.130	1.34
4.1	1.304	1.10
5.3	1.683	1.10
1.8	0.737	1.42
0.8	0.278	1.20
2.4	0.934	1.34
3.5	1.113	1.10

$\bar{u} = 7.67 \times 10^3$ cm s^{-1}, $t = 2.89 \times 10^{-3}$ s.

k(2) corr = $(1.4 \pm 0.5) \times 10^{-12}$ cm^3 s^{-1}[a]

[a]This rate constant is the product of the correction factor of 1.3 and the slope of the unweighted least squares fit to the data in columns (1) and (2) above. The error reflects the statistical uncertainty (1σ) and the uncertainty introduced by using the mean correction factor.

TABLE 9. KINETIC DATA FOR THE $N(^2D) + H_2$ STUDY (2)

(1) $[H_2]$ ($\times 10^{14}$ cm^{-3})	(2) $\ln\left(\frac{k_0 l_{(max)}}{k_0 l_{(H_2)}}\right)$	(3) k(2) ($\times 10^{-12}$ cm^3 s^{-1})
0.60	0.339	1.89
1.12	0.562	1.68
2.10	1.362	1.68
1.83	0.939	1.72
1.50	0.637	1.42
0.71	0.616	2.91
0.14	0.122	2.92
1.10	0.828	2.52

$\bar{u} = 7.67 \times 10^3$ cm s^{-1}, $t = 2.89 \times 10^{-3}$ s.

k(2) corr = $(2.3 \pm 0.8) \times 10^{-12}$ cm^3 s^{-1} (1σ)[a].

[a]This rate constant is the product of the correction factor of 1.3 and the slope of the unweighted least squares fit to the data in columns (1) and (2) above. The error reflects the statistical uncertainty (1σ) and the uncertainty introduced by using the mean correction factor.

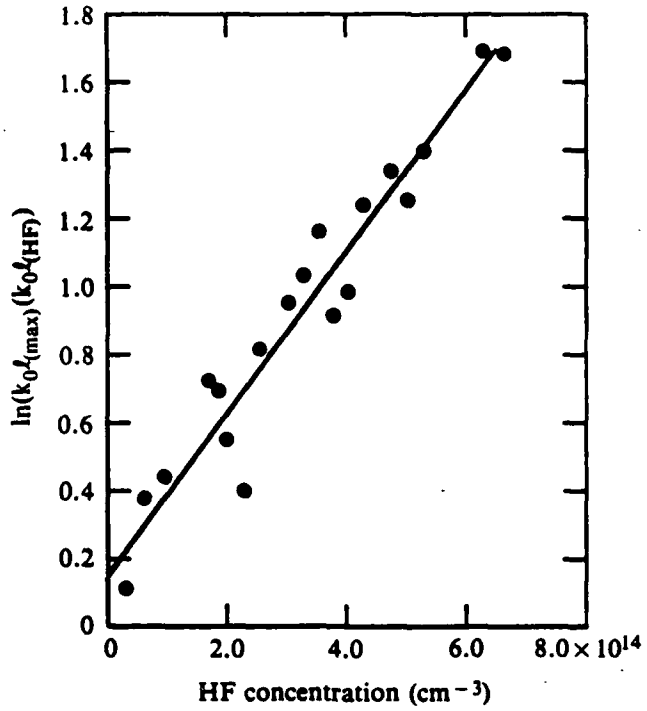

Figure 20. Typical pseudo-first-order kinetic data for the N(²D) + HF study.

e. Discussion--The measurement of $N(^2D)$ atom reaction rate-constants in a fast-flow reactor with a microwave discharge of N_2 in a carrier gas (Ar) as the source of N atoms may be complicated by side reactions arising from discharge products (other than $N(^2D)$ atoms). These discharge products will invalidate the pseudo-first-order kinetic analysis used. The principal species of concern are metastable molecular nitrogen ($N_2(A^3\Sigma_u^+)$), metastable argon ($Ar(^3P)$), and ground-state nitrogen atoms, ($N(^4S)$). Metastable $N_2(A)$ molecules are expected to be in low concentration and not to survive for more than a few centimeters downstream of the discharge. They are mainly produced via the termolecular recombination of $N(^4S)$ atoms, a process with a rate constant of $\sim 10^{-17}$ cm^3 s^{-1}, and are also rapidly quenched on collision with $N(^4S)$ atoms (Ref. 47). Typical concentrations of $N(^4S)$ atoms produced in the discharge are $\sim 10^{14}$ cm^{-3}. The concentration of $Ar(^3P)$ atoms produced in a microwave discharge under similar conditions employed in these studies is found to be so small compared to the concentrations of O_2, H_2, and HF that any loss of reagent due to $Ar(^3P)$ can be neglected (Ref. 34). The reactions of

TABLE 10. KINETIC DATA FOR THE $N(^2D) + HF$ STUDY

(1) [HF] ($\times 10^{14}$ cm^{-3})	(2) $\ln\left(\frac{k_0^l(max)}{k_0^l_{HF}}\right)$	(3) k(3) ($\times 10^{-13}$ cm^3 s^{-1})
3.24	1.03	10.60
1.99	0.55	9.21
0.92	0.43	15.55
0.60	0.38	21.11
0.27	0.11	13.50
6.24	1.69	9.02
5.23	1.40	8.92
4.23	1.24	9.77
3.00	0.95	10.55
2.26	0.41	6.05
3.49	1.16	11.08
6.65	1.69	8.47
3.79	0.92	8.09
2.51	0.82	10.88
1.66	0.73	14.84
4.72	1.34	9.46
3.98	0.98	8.02
1.88	0.70	12.61
0.00	0.00	

$\bar{u} = 7.33 \times 10^3$ cm s^{-1}, $t = 3.0 \times 10^{-3}$ s.

k(3) corr = $(1.1 \pm 0.3) \times 10^{-12}$ cm^3 s^{-1}.[a]

[a]This rate constant is the product of the correction factor of 1.3 and the slope of the unweighted least squares fit to the data in columns (1) and (2) above. The error reflects the statistical uncertainty (1σ) and the uncertainty introduced by using the mean correction factor.

$N(^4S)$ atoms with O_2 and H_2 are found to be too slow to affect the pseudo-first-order kinetic analysis. There appears to be no reported measurement of the rate constant for the reaction of $N(^4S)$ atoms with HF; however, from thermochemical considerations, any such reaction would be significantly endothermic and, thus, this reaction is also considered to be unimportant in the $N(^2D)$ atom kinetics described. The excellent agreement between k(1)corr measured in this study and those values reported in the literature (Table 7) indicated that the experimental system used was free of systematic errors and was suitable to be used in the measurement of k(2)corr and k(3)corr. The value of k(2)corr measured in this study agrees within experimental error with all other reported values with the exception of an early photolysis experiment measurement by Black et al. (Ref. 8). It is reasonable, therefore, to have

continued confidence in the rate recommended by Schofield (Ref. 11), which has been used in the flame-modeling package to date. The rate constant k(3)corr is similar in magnitude to that for the analogous H_2 reaction and would be expected to compete in a similar manner for the $N(^2D)$ atoms generated in the H + NF_2 flame. No attempt has been made to identify whether the depletion of $N(^2D)$ atoms in the H_2 or HF reactions was via a quenching or a reactive channel.

2. *THE RATE CONSTANT FOR THE REACTION OF* $N(^2D)$ *ATOMS WITH NF(a),*
$N(^2D) + NF(a) \rightarrow N_2(B,W) + F(^2P)$

a. Introduction--The rate constant for the production of $N_2(B,W)$ molecules from the reaction of $N(^2D)$ atoms with NF(a), k_p, can be determined by assuming the steady-state condition

$$\{d[N_2(B,W)]/dt\}_{ss} = k_p\,[N(^2D)][NF(a)] - [N_2(B)]/\tau_{rB} = 0 \qquad (37)$$

where $[N(^2D)]$, [NF(a)], $[N_2(B)]$ and $[N_2(B,W)]$ are the absolute concentrations of $N(^2D)$ atoms, $NF(a^1\Delta)$ radicals, $N_2(B)$ molecules and the $N_2(B)$ plus $N_2(W)$ manifold, respectively, and τ_{rB} is the effective radiative lifetime of the total $N_2(B)$ concentration. This equation is derived from the assumptions that reaction (38) is the only process generating $N_2(B,W)$ in the H + NF_2 flame and that reaction (39) is the predominant loss channel for $N_2(B)$ (Ref. 48),

$$N(^2D) + NF(a^1\Delta) \rightarrow N_2(B,W) + F \qquad (38)$$

$$N_2(B) \rightarrow N_2(A) + h\nu \qquad (39)$$

It is important to appreciate that the loss term $[N_2(B)]/\tau_{rB}$ uses only the $N_2(B)$ concentration since radiative losses of $N_2(W)$ are negligible (Ref. 7).

b. Experiment--The flow tube apparatus is schematically represented in Figure 21. The apparatus is a modification of the apparatus shown in Figure 16 with a resonance lamp, absorption cell, and monochomator system at the

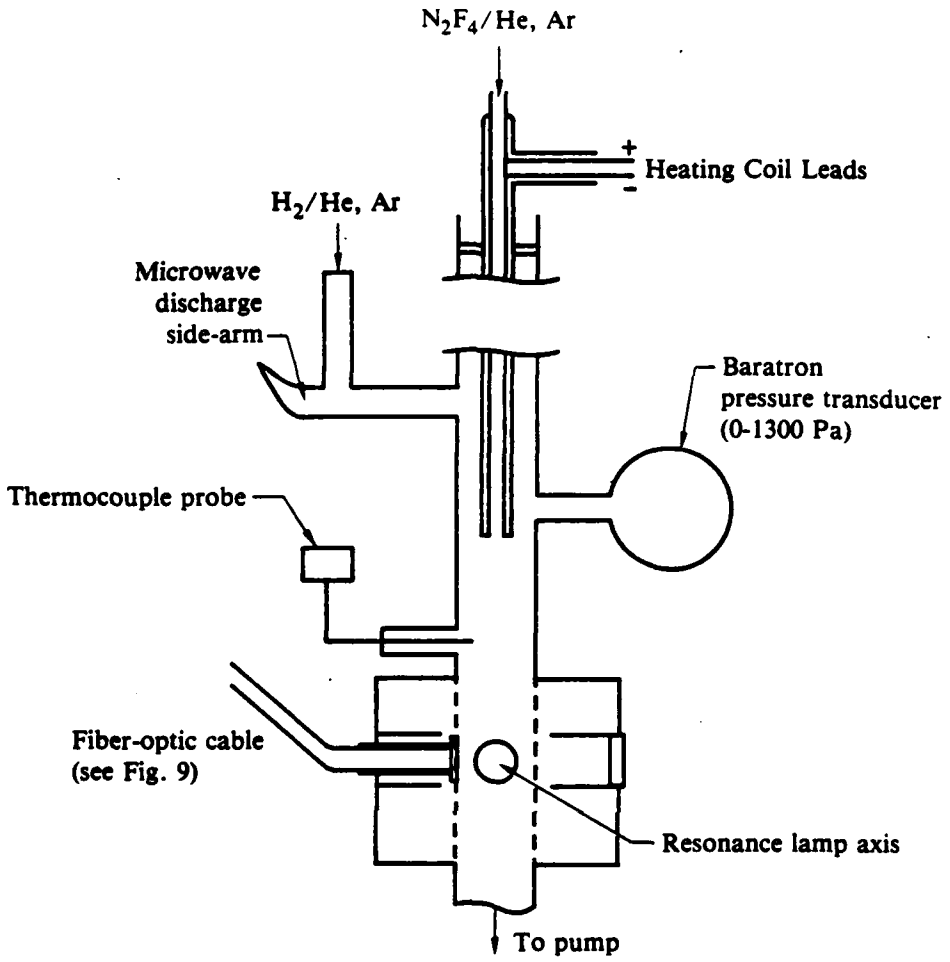

Figure 21. Flow tube for the N(^{2}D) + NF(a) studies.

fixed observation point for monitoring N(^{2}D) atoms generated in the H + NF_2 flame. Hydrogen atoms were generated upstream in the flow tube (in the side arm microwave discharge) by a 2.45-GHz microwave discharge in either pure H_2 or a dilute mixture of H_2 in He (typically 1% H_2 in He). The NF_2 radicals were generated by thermal decomposition of N_2F_4 diluted in He. The mixtures of N_2F_4 in He were prepared in the N_2F_4 remote handling facility (Appendix I). Mixture ratios ranged from 1:1 to 1:200, N_2F_4:He. Thermal decomposition of the N_2F_4 was achieved in the flow tube by flowing the N_2F_4/He mixture through the heated injector. A detailed design of the heated injector used for these studies is given in Figure 22. The heated injector was designed to be both easily movable along the longitudinal axis of the flow tube and to remain in concentric alignment with the longitudinal axis of the flow tube. The

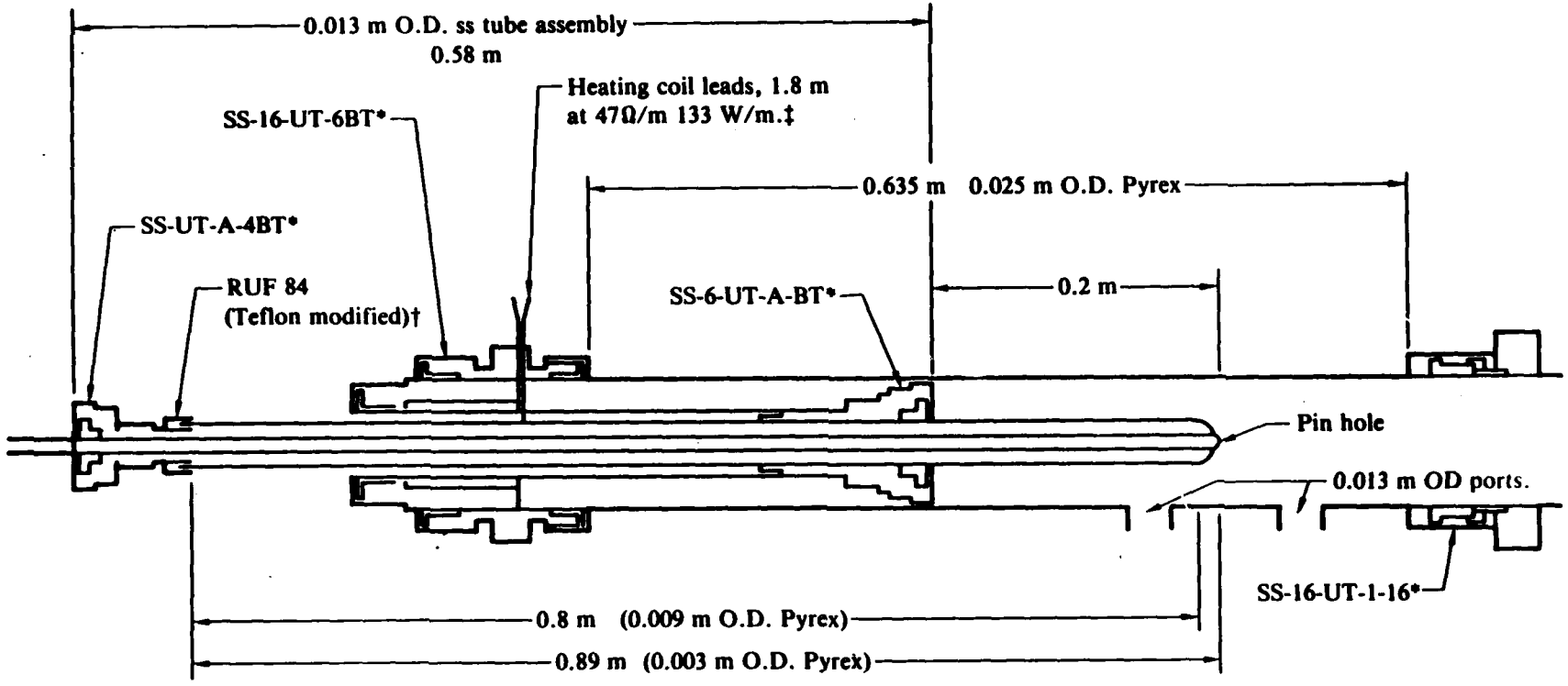

*Part numbers for "ultratorr" s.s. vacuum unions.
†"Nacom" teflon vacuum union.
‡Clayborn Labs Inc. Part number E-16-24.

Figure 22. Free-moving, heated- injector design and specifications.

mobility of the heated injector was required to vary the reaction time which was calculated from the flow velocity of the reaction mixture through the flow tube and the distance between the end of the heated injector and the centerline of the fixed observation point. To ensure thermal equilibrium throughout the heated section of the injector, the power to the injector heating element was established at least 2 hours before any experiment. The internal surface of the flow tube and the external surface of the heated injector were coated with halocarbon wax to minimize losses of H atoms on the walls.

The optical emission measurements were made with the PAR model 1420 intensified diode array cooled to -25°C. Acquisition and analysis of the data were performed with a PAR Model 1460 optical multichannel analyzer (OMA) console as described in Section III, paragraph 3.b. Optical emission from the flow tube at the fixed observation point was collected through an internally mounted window aligned perpendicular to both the flow tube longitudinal axis and the resonance absorption experiment axis (Fig. 23). The internally mounted window provided for optimum light collection from the flow tube

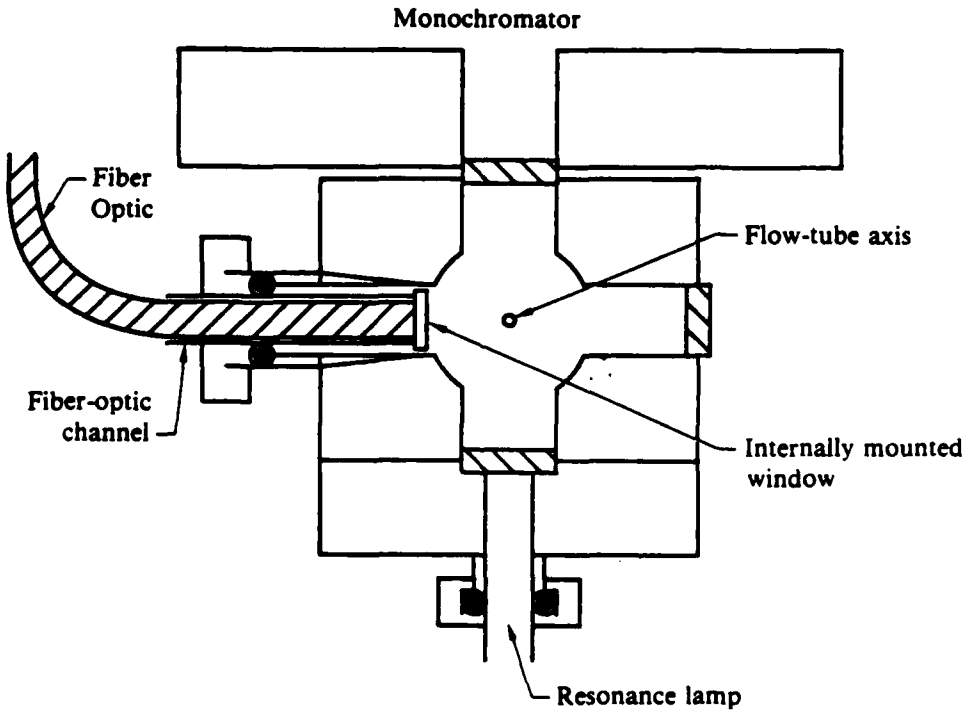

Figure 23. Cross section of fixed observation point showing internally mounted window for optimum optical-emission collection.

without modifying the absorption cell at the fixed observation point. The emission was transmitted to the entrance slits of the OMA monochromator through a 0.64-m fiber-optic cable. All the optical emissions to be monitored in this experiment were in the region of 870 ± 20 nm. To minimize the problem of short-wavelength emissions in second order and background-scattered light, a long-pass filter (Schott Glass Filter RG780) was placed between the fiber-optic cable and the entrance slits. The absolute concentrations of NF(a) and $N_2(B)$ were derived from the optical emission experiments by an absolute spectrophometric calibration of the optical-emission collection and detection system. Calibration was performed with the O + NO reference-emission technique described in Section III, paragraph 2.a, c, and e. Oxygen atoms were generated by a microwave discharge through a mixture of O_2 in carrier gas, in the discharge side arm. The NO_2 (Matheson, 99.5%) was used without further purification to titrate the O atoms generated in the discharge and to generate the reference emission.

c. Results--The $N_2(B)$ and NF(a) concentrations were determined by deconvolving their respective emission spectra as described in Sections III, paragraphs 2.a, c, and e. The $N(^2D)$ atom concentrations were determined from atomic-resonance-absorption measurements as described in paragraph 1.b.

Four independent measurements of the rate constant k_p were made with the steady-state analysis. The experimental conditions and results for each experiment are presented in Table 11. The measurements were made with two different mixtures of N_2F_4 in He. Two of the measurements (experiments 1 and 4 of Table 11) were made with differing mixtures of N_2F_4 in He by adjusting the position of the heated injector to yield a reaction time such that the peak $N_2(B-A)$ emission was detected at the fixed observation point. The other two measurements were made at reactions times slightly before and after the peak of the $N_2(B-A)$ emission. (These experiments were performed under the same conditions as experiment number 1). In all experiments k_p was found to be $\sim 1 \times 10^{-10}$ cm^3 s^{-1}.

d. Discussion--The small stoichiometric range over which the system was studied and the uncertainties associated with the calculation of the $N(^2D)$, NF(a) and $N_2(B)$ concentrations require that this measurement should be considered an estimate of the $N(^2D)$ + NF(a) reaction rate constant. As such, the

TABLE 11. DATA FOR STEADY-STATE EVALUATION OF k_p

Experiment No.	$[NF(a^1\Delta)]$ (cm^{-3})	$[N_2(B)\ v=2]$ (cm^{-3})	$[N_2(B_{total})]$ (cm^{-3})	$[N(^2D)]^d$ (cm^{-3})	Δt (10^{-3} s)	$k_p{}^c$ ($cm^3\ s^{-1}$)
[a]1	8.67×10^{12}	2.06×10^{8}	1.88×10^{9}	3.0×10^{11}	2.0	1.2×10^{-10}
[a]2	4.33×10^{12}	0.49×10^{8}	0.45×10^{9}	2.6×10^{11}	4.0	0.7×10^{-10}
[a]3	6.57×10^{12}	1.39×10^{8}	1.27×10^{9}	3.3×10^{11}	3.0	1.0×10^{-10}
[b]4	1.86×10^{13}	2.72×10^{8}	2.48×10^{9}	2.3×10^{11}	1.9	1.0×10^{-10}

[a]Experimental conditions for experiments 1 - 3.
$[N_2F_4] = 1.05\times10^{14}\ cm^{-3}$, $[H_2] = 3.43\times10^{14}\ cm^{-3}$, $[He] = 1.75\times10^{16}\ cm^{-3}$

[b]Experimental conditions for experiment 4.
$[N_2F_4] = 6.2\times10^{14}\ cm^{-3}$, $[H_2] = 6.96\times10^{14}\ cm^{-3}$, $[He] = 1.94\times10^{16}\ cm^{-3}$

[c]$k_p = \dfrac{[N_2(B)]}{\tau_{rB}\cdot[N(^2D)]\,[NF(a^1\Delta)]}$, where $\tau_{rB} = 6.02\times10^{-6}$ s

[d]$[N(^2D)] = 2.67\times10^{11}\times k_0 l\ /f_{Lu} l$, where $l = 2.5$ cm, $f_{Lu} = 0.052$

rate constant is quoted with no error limits. Considering all the factors it would be unlikely that the true rate constant for the $N(^2D)$ + NF(a) reaction would differ by more than a factor of 2 from the estimate determined in this work.

The important conclusion of this study is that the $N(^2D)$ + NF(a) reaction is extremely fast and is not a rate-limiting step for the generation of $N_2(A)$ in the H + NF_2 system.

3. RATE CONSTANT FOR THE QUENCHING OF $N_2(A)$ BY H ATOMS

a. Introduction and background--The results of the $N_2(A)$ and $N_2(B)$ population profiles, reported in Sections III, paragraphs 4.c and e, indicated that there exists an $N_2(A)$ loss channel that is significantly faster than wall quenching. This loss channel, quenching by H atoms, was identified by the following experiment. Using the metastable transfer source for $N_2(A)$ described in Section III, paragraph 3.a (no NF_2 was added), the spectrum in Figure 24 labeled No H atoms was obtained. Adding an H_2 flow to the microwave discharge in He to yield an H-atom concentration < $10^{13}\ cm^{-3}$ resulted in the spectrum labeled H atoms present (Fig. 24). The $N_2(A)$ intensities under these conditions are considerably reduced. Such results imply a quenching rate-constant greater than $5\times10^{-12}\ cm^3\ s^{-1}$ (Ref. 49). Given the impact such a rate has on the use of the H + NF_2 system in an $N_2(A)$ generator, a more

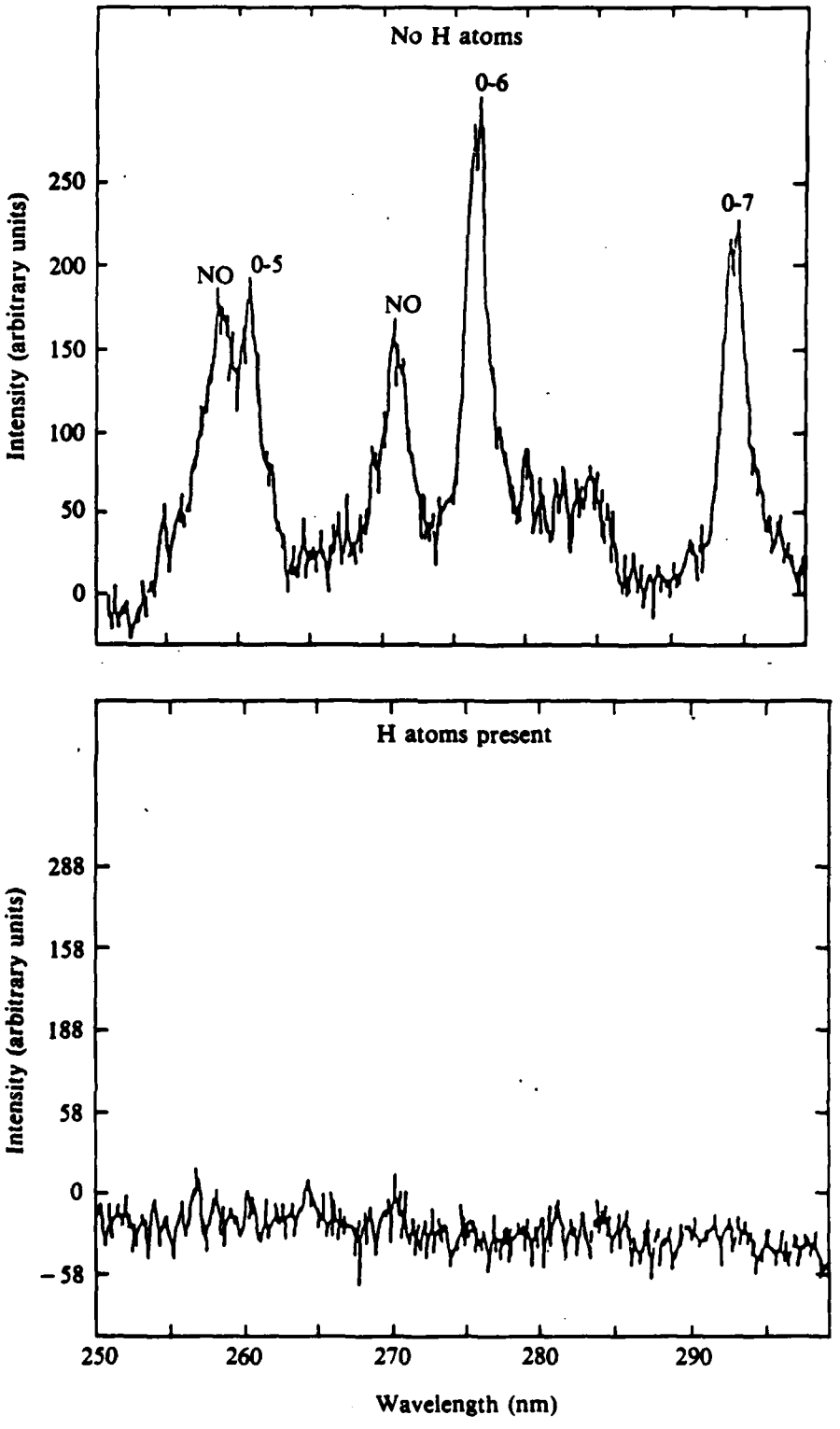

Figure 24. Spectra of $N_2(A)$, with and without H atoms.

precise determination of the rate constant for $N_2(A)$ quenching by H atoms was performed.

The approach used was to measure the decrease in the $N_2(A)$ emission signal for a known H-atom concentration at a fixed time from the mixing point of the two reactants. In all cases [H] >> [$N_2(A)$] so that pseudo-first-order kinetics applied. The H-atom concentration was determined by titration with NO_2 (Ref. 50). The low [H]s used (< 10^{13} cm^{-3}) did not allow the determination of the endpoint by the observation of HNO recombination emission. Instead, NF_2 was added at the observation region and the resulting NF(b) emission at 529 nm used as an endpoint indicator.

b. Experiment--The same basic flow system used previously for the population profiles was used in these measurements (Fig. 2 and Section III, paragraph 3.a). The principal difference was the removal of the chemical trap which resulted in an increase in flow velocity. The microwave discharge in He, to which H_2 was added as needed, was 0.53 m upstream of the optical observation port. The Ar metastable transfer source for $N_2(A)$ was 0.38 m upstream of the optical port. A fixed injection tube located 0.25 m upstream of the optical ports was used to add NO_2 for the H-atom titration. One of the observation ports was modified to accept a heated (~ 200°C) Pyrex injector through which ~1% mixtures of N_2F_4 in He could be added to generate NF_2. For all quenching measurements the Ar flow was 1.78 x 10^{21} molecules s^{-1}, the N_2 flow was 5.24 x 10^{20} molecules s^{-1}, and the He flow was 1.34 x 10^{21} molecules s^{-1}, giving a total pressure of 69 Pa and a flow velocity of 4430 cm s^{-1}. The H_2 flows ranged from (3-13) x 10^{17} molecules s^{-1} and had a negligible effect on the total pressure or flow velocity. For the H-atom titrations, the same conditions as the corresponding quenching measurement were used with the addition of an N_2F_4/He mixture flow of 6.1 x 10^{19} molecules s^{-1} through the heated injector to monitor the titration end point. The heated injector was mounted perpendicular to the main flow tube, directly opposite the detector used for recording all emission spectra.

The OMA III intensified-diode-array detection system (Section III, paragraph 3.b) was used to record both the $N_2(A)$ emission for the quenching measurements and the NF(b) emission for the H-atom titrations. Five-minute background-subtracted scans of the $N_2(A-X,0-6)$ emission at 276 nm were used to determine relative [$N_2(A,v=0)$]s. The NF(b) relative concentration

measurements required 20- to 60-s background-subtracted scans of the 529-nm NF(b-X) emission, depending upon the concentration of H atoms being titrated.

c. Data analysis--The determination of the rate constant for $N_2(A)$ quenching by H atoms involves two primary steps: (1) the determination of the concentration of H atoms and (2) the pseudo-first-order kinetic analysis of the $N_2(A)$ relative concentration data. Because of the low H-atom concentrations used (10^{12} cm^{-3} → 10^{13} cm^{-3}) and the relatively high flow-velocity, the apparent endpoint of the NO_2 titration (i.e., the NO_2 flow for which the NF(b) emission at the observation port disappears) does not occur when the added $[NO_2]$ equals $[H]_o$. A full second-order kinetic analysis of the titration data must be performed to determine the true endpoint. The analysis of the $N_2(A)$ relative concentration data to extract the quenching-rate constant involves standard pseudo-first-order analysis.

(1) H-atom titration analysis--The determination of H-atom concentrations by titration with NO_2

$$H + NO_2 \rightarrow NO + OH,\ k_{298} = 1.3\times10^{-10}\text{cm}^3\ \text{molecules}^{-1}\ \text{s}^{-1} \qquad (40)$$

has been discussed in the review chapter by Clyne and Nip (Ref. 50). The low H-atom concentrations (10^{12} -10^{13} cm^{-3}) and short reaction time (5.6 ms) used in these measurements will avoid the interference of the secondary reactions of OH that they discuss.

One difficulty, mentioned earlier, is that under the conditions of these studies, the titration reaction can be as little as 50% complete at the observation port. The results can be analyzed by applying the well-known results for second-order reactions (Ref. 51) to the $H + NO_2$ system to give

$$\ln([H][NO_2]_0/[H]_0[NO_2]) = kt([H]_0-[NO_2]_0) \qquad (41)$$

where k is the rate constant for the $H + NO_2$ reaction, $[H]$ and $[NO_2]$ are the H-atom and NO_2 concentrations at time t, and $[H]_0$ and $[NO_2]_0$ are the initial H-atom and NO_2 concentrations. This can be rewritten as

$$R = \frac{(1 - [H]_0/[NO_2]_0)}{(e^{kt([NO_2]_0 - [H]_0)} - [H]_0/[NO_2]_0)} \quad (42)$$

where $R=[H]/[H]_0$. To determine a particular $[H]_0$, R was measured as a function of $[NO_2]_0$. By numerically fitting the results to Equation 42, the best estimate for $[H]_0$ was found.

The values of R are determined from the intensity of NF(b) emissions resulting from the H + NF_2 indicator reaction at the observation port. It has been shown that this reaction possesses a direct channel which forms NF(b) (Ref. 3). Since the time for reaction between the residual H atoms and the NF_2 injected at the observation is short, secondary reaction formation of NF(b) is negligible. As a result, the intensity of NF(b) emission for a particular $[NO_2]_0$ in the titration is directly proportional to the residual H-atom concentration at the observation port. Thus, the values of R are determined simply by dividing the NF(b) emission intensity at a particular $[NO_2]_0$ in the titration by the initial NF(b) intensity (i.e., the intensity before addition of NO_2).

(2) $N_2(A)$ quenching kinetics--Because the H-atom concentrations were 10^{12} -10^{13} cm^{-3} for all experiments and the $N_2(A)$ concentration was less than 10^{10} cm^{-3} (Section III, paragraph 4.e), pseudo-first-order analysis applies. Thus, for a known initial $[H]_0$,

$$\ln([N_2(A)]_0/[N_2(A)]) = k_q[H]_0 t \quad (43)$$

where k_q is the quenching rate constant, $[N_2(A)]_0$ is the initial $N_2(A)$ concentration, and $[N_2(A)]$ is the concentration at time t. In the measurements, the ratio $[N_2(A)]_0/[N_2(A)]$ was obtained from the ratio of the $N_2(A\text{-}X,0\text{-}6)$ emission intensity at the observation port without H atoms to that with H atoms. Since $[H]_0$ and t are known, k_q can be calculated. In all cases, the simple plug-flow model was assumed.

d. Results and discussion--The rate constant k_q was determined for seven different $[H]_0$s. For each $[H]_0$, three separate measurements of the $[N_2(A)]_0/[N_2(A)]$ ratio were made by alternately recording the $N_2(A\text{-}X,0\text{-}6)$ emission spectrum with and without H_2 added to the microwave discharge. After

the $N_2(A)$ population ratio measurements were made, the $[H]_0$ was determined by titration with NO_2. The results, summarized in Table 12, yield a value for k_q of $5.1 \pm 1.5 \times 10^{-11}$ cm^3 s^{-1}, where the uncertainty represents the standard deviation of a single measurement from the mean. This value is consistent with the lower-limit measurement (Ref. 49). The scatter in the measured values of k_q can largely be explained by the uncertainties in the determination of the $[H]_0$s.

Clearly, such a large quenching rate constant seriously constrains the conditions under which the $H + NF_2$ reaction can be efficiently used to produce $N_2(A)$. Competition for NF(a) by channels other than reaction (2) cannot be overcome simply by increasing $[H]_0$. A detailed kinetic modeling study will be necessary to determine the optimum conditions for $N_2(A)$ production and subsequent energy transfer to a potential laser candidate.

TABLE 12. RESULT OF $N_2(A)$ QUENCHING BY H ATOMS

$[H]_0$ (10^{12} cm^{-3})	2.0	4.4	2.0	2.2	4.1	3.1	0.82
k_Q (10^{-11} cm^3 s^{-1})	3.2	3.9	6.4	5.9	4.2	7.4	4.8

k_Q (average) = $(5.1 \pm 1.5) \times 10^{-11}$ cm^3 s^{-1}

V. MODULATED-BEAM MASS SPECTROMETRIC INVESTIGATIONS OF N_2F_4 THERMAL DISSOCIATION

1. INTRODUCTION

A major uncertainty in using heated N_2F_4 as a source for NF_2 is the assumption of 100% dissociation of the N_2F_4 at the pressures and temperatures encountered in the source injector. Thermodynamic calculations based on the equilibrium constant for the equilibrium reactions,

$$N_2F_4 \rightleftarrows NF_2 \tag{45}$$

show that N_2F_4 is fully dissociated under the conditions encountered in experiments described in this report (Ref. 52). These calculations do not truly represent equilibrium conditions, however, since they do not consider all possible chemical species. As shown in Table 13, a true equilibrium calculation (using the Gordon McBride equilibrium code [Ref. 53]) predicts N_2, F_2, and NF_3 to be the predominant species present.

Quantitative production of NF_2 from a heated N_2F_4 source is possible, however, primarily because of the large difference in N-N and N-F bond strengths. The N-N bond strength in N_2F_4 is 92 kJ/mol, whereas a typical bond strength for N-F is much larger (e.g., 252 kJ/mol for NF_3). The kinetic processes (gas-phase and wall reactions) for breaking N-F bonds are, therefore, more endothermic (hence, slower) than the analogous processes for breaking N-N bonds.

Thus, it is possible to design a thermal dissociator for N_2F_4 that will produce NF_2 as the predominant product; however, care must be taken to allow sufficient time for the N_2F_4, NF_2 equilibrium to be established without allowing subsequent NF_2 dissociation to occur. Therefore, the experiments were undertaken to characterize the thermal sources of NF_2 used in the kinetic studies.

2. EXPERIMENT AND RESULTS

The EPR, OES, Modulated Beam Mass Spectrometric, (MBMS) flow reactor was used to investigate the thermal dissociation of N_2F_4. In these investigations, a mixture of N_2F_4 in He was injected into the flow reactor after passage through a heated tube. At a position approximately 0.2 m from the injection point, a small fraction of the mixture passed through a skimmer

TABLE 13. EQUILIBRIUM COMPOSITION OF N_2F_4 AT 500 K[a]

	Pressure (Pa)			
	1.3	13	130	1300
NF_3	0.67	0.77	0.79	0.80
N_2	0.22	0.20	0.20	0.20
F_2	0.10	0.03	0.01	0.001
F	—	—	—	—
NF_2	—	—	—	—

[a]NASA Technical Report SP-273, S. Gordon and B.J. McBride, NASA Scientific and Technical Int. Office, Washington, D.C., 1971.

into a diffentially-pumped, high-vacuum system where the effluent was analyzed with a modulated-beam mass spectrometer.

In the first series of experiments, a glass probe made of quartz and Pyrex glass (Fig. 25) was investigated. Figure 26 is a typical mass spectrum, obtained upon heating the probe to temperatures near 250°C. It can be readily seen that the effluent from the heated source was completely dissociated at this temperature (as shown by the absence of the parent peak for N_2F_4 at a mass-to-charge ratio (m/e) of 104) but the mixture was contaminated by oxide species as well as NF_2. Experiments were initiated to determine the nature of the oxide species in the flow; however, during the course of these experiments (over a period of 2-4 hours of running time) the oxide peaks diminished in intensity, finally becoming undetectable. These results indicate that the oxides form by reaction of NF_2 with the glass probe surfaces but that with time these surfaces eventually passivate when exposed to NF_2 rendering subsequent wall reaction losses of NF_2 negligible.

Because the possibility of NF_2 reacting with the glass surfaces was raised, however, a heated metal probe for producing NF_2 was fabricated and further experiments were performed to characterize this probe. Figure 27 shows the design for this stainless steel probe.

The results of the characterization of the stainless steel injector are shown in Figure 28. Every major mass peak obtained at 200°C can be attributed to a cracking peak obtained during electron bombardment ionization of NF_2.

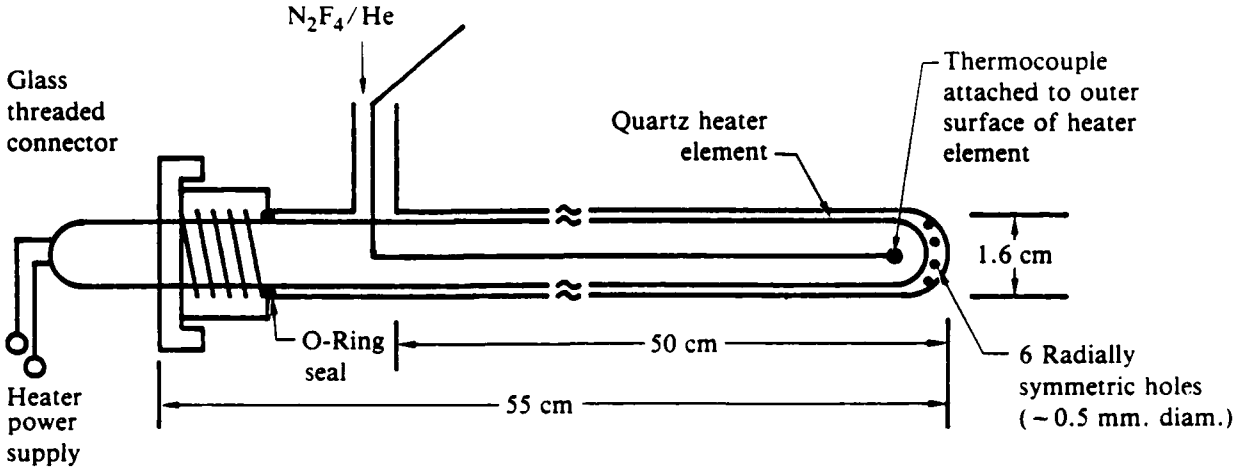

Figure 25. Glass probe design and specifications.

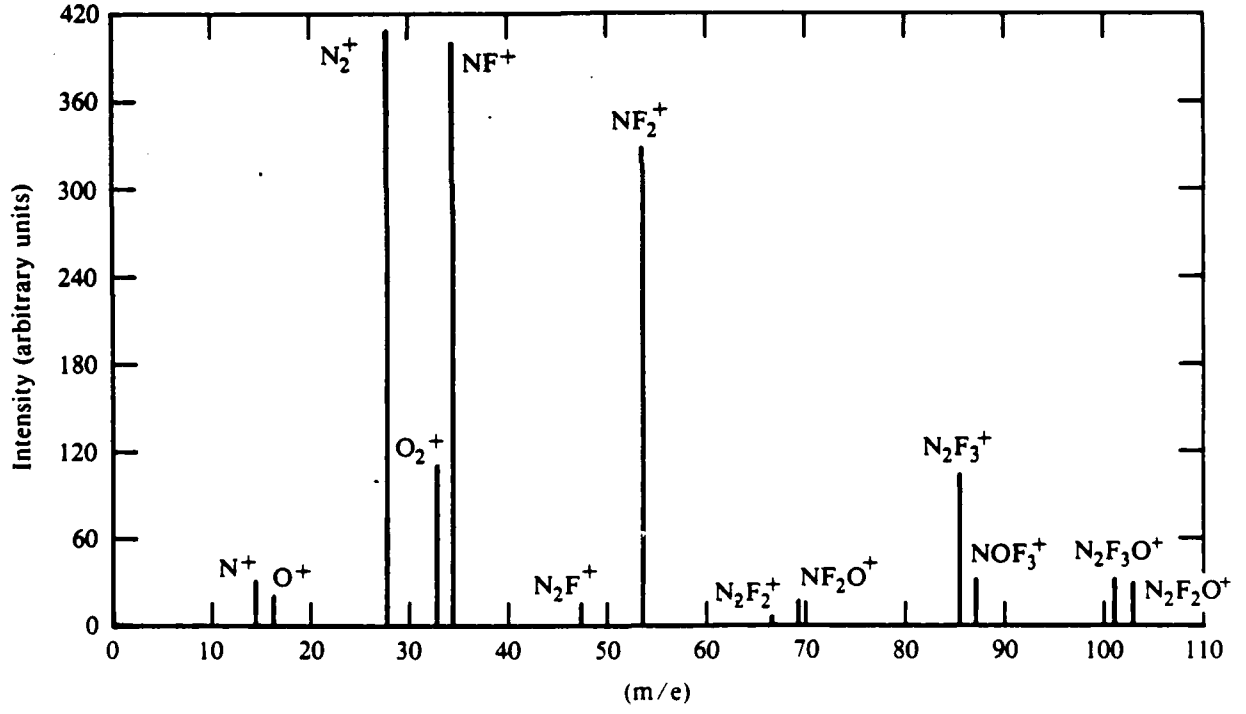

Figure 26. Mass spectrum of glass probe effluent at 250°C, recorded before passivation had taken place.

The small cracking peaks at masses corresponding to N_2F^+ and $N_2F_2^+$, which are also found in the room-temperature mass spectrum, can be attributed to a small N_2F_2 impurity in the N_2F_4 sample. The N_2F_2 has previously been identified as an impurity in the N_2F_4 used in these studies by gas chromatographic analysis

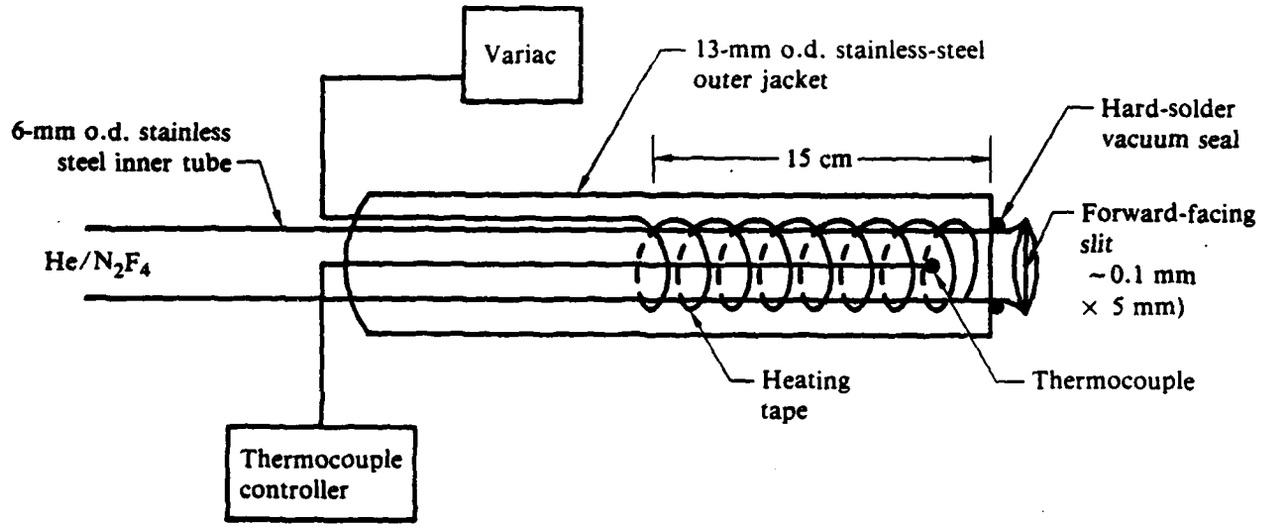

Figure 27. Metal probe design and specifications.

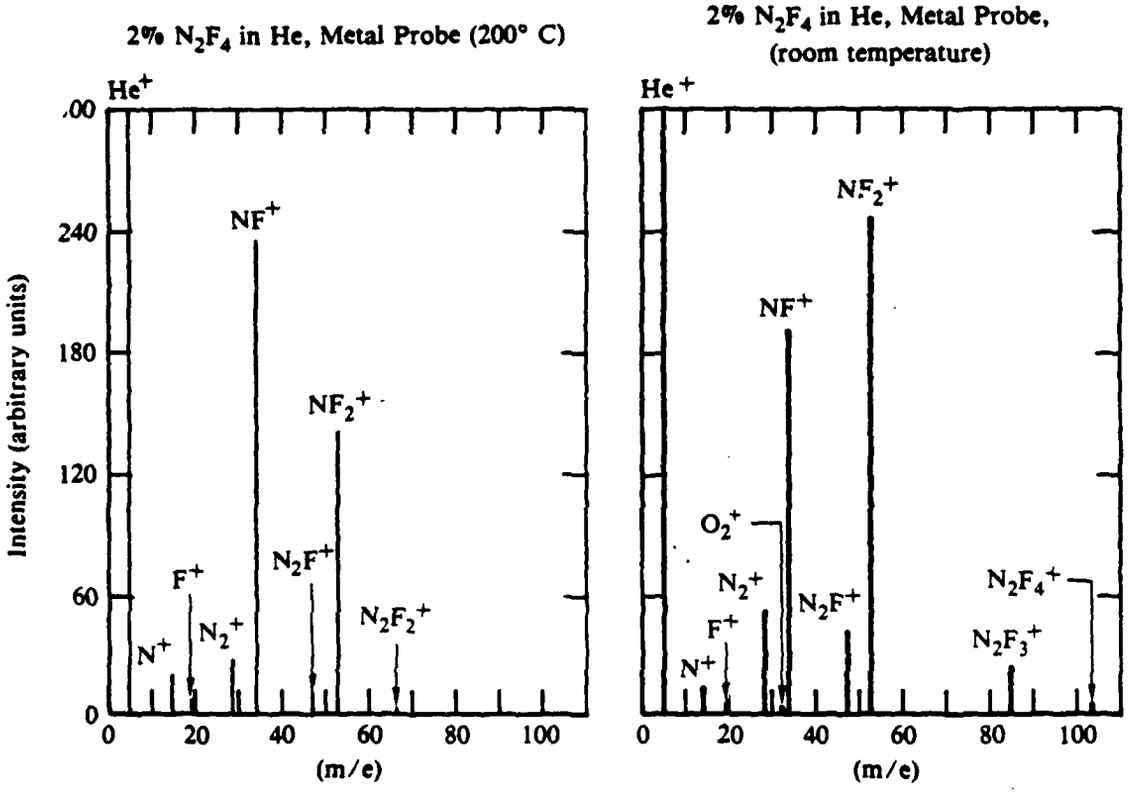

Figure 28. Mass spectra of metal probe effluent recorded at 200°C and at room temperature

(Ref. 54). Thus, the absence of the parent N_2F_4 peak indicates nearly complete dissociation (> 95%) at this temperature and the absence of any major impurity peaks indicates that the effluent from the source is primarily NF_2.

VI. CONCLUSIONS

The peak NF(a) populations based on OES measurements are only 15-20% of predicted yields based on complete conversion of N_2F_4 to NF(a). Measured $N_2(B)$ production efficiencies (assumed to be a lower limit on $N_2(A)$ productic efficiency) range from 3-25% depending whether they are referenced to concentration of N_2F_4 consumed or peak NF(a) concentrations measured. Profiles of the NF(b) and $N_2(A)$ populations were determined. For the conditions of these measurements (relatively low H_2 and HF(v>2) concentrations), the peak NF(b) concentrations were more than two orders of magnitude lower than NF(a) concentrations, indicating that NF(a) pooling with HF(v≥2) to give NF(b) is not a significant loss channel. Due to signal-to-noise constraints, only upper limits on $N_2(A)$ concentrations produced in the H + NF_2 system could be determined. These limits are consistent with $N_2(A)$ formation by radiative decay of $N_2(B)$ and loss by a channel significantly faster than wall quenching.

The rate constants for a number of processes involved in the H + NF_2 system were determined. The reaction of $N(^2D)$ with NF(a) to form $N_2(B,W)$ was found to to be an extremely fast process with a rate constant of ~1 x 10^{-10} cm^3 s^{-1}. The competing reactions with H_2 and HF were much slower, having rate constants of 1.8 x 10^{-12} cm^3 s^{-1} and 1.0 x 10^{-12} cm^3 s^{-1}, respectively. Under the conditions of the measurements of the H + NF_2 system these latter reactions would not represent significant loss channels for the $N(^2D)$. A fast $N_2(A)$ loss channel was found to be quenching by H atoms and to have a rate constant of 5.1 x 10^{-11} cm^3 s^{-1}. Such a fast removal of $N_2(A)$ by H atoms prevents the build-up of high $N_2(A)$ concentrations in the H + NF_2 system.

To efficiently extract the $N_2(A)$ energy, therefore, a transfer partner would have to meet a number of criteria. In particular, the transfer partner must be premixed with the H + NF_2 flame precursors, it must be added in sufficiently high concentration to compete with the H-atom loss channel, and it must not interfere or be depleted by the chemistry that generates the $N_2(A)$.

VII. RECOMMENDATIONS

The peak NF(a) populations are only 15-20% of what would be expected assuming complete conversion of input N_2F_4 to NF(a). This is an important issue that needs to be resolved to accurately assess the use of the H + NF_2 system for the generation of $N_2(A)$. In particular, the measured $N_2(B)$ production efficiencies (which are a lower limit on $N_2(A)$ production efficiencies) range from ~3-25%, depending upon whether they are referenced to input N_2F_4 or to peak NF(a) concentrations. Critical parameters that affect the OES measurements and should be remeasured are the NF(a) radiative lifetime, the radiative rate constant for the reference O + NO reaction, and the branching ratio for the H + NF_2. It is also possible that an as yet unidentified NF(a) loss channel is causing the low NF(a) peak concentrations and disproportionation of the input NF_2 within the heated injector could also cause lowered NF(a) yields under some circumstances. It is recommended, therefore, that these issues also be addressed in future studies associated with the understanding of $N_2(A)$ generation in the H + NF_2 system.

REFERENCES

1. Cheah, C. T. Clyne, M. A. A., and Whitefield, P. D., "Reactions Forming Electronically Excited Free Radicals, Part 1," J. Chem. Soc. Faraday Trans. II, 76, 711 (1980).
2. Cheah, C. T., and Clyne, M. A. A., "Reactions Forming Electronically Excited Free Radicals, Part 2, J. Chem. Soc. Faraday Trans. II, 76, 1543 (1980).
3. Malins, R. J., and Setser, D. W., "Rate Constants, Branching Ratios and Energy Disposal for NF(a,b,X) and HF(v) Formation From the H + NF_2 Reaction, J. Phys. Chem. 85, 1342 (1981).
4. Cheah, C. T., and Clyne, M. A. A., "Reactions Forming Electronically Excited Free Radicals III," J. Photochem. 15,21 (1981).
5. McDonald, R. G., and Sloan, J. J., "Microscopic V-E Energy Transfer Rates in the HF/NF System," Chem. Phys. Lett. 61, 137 (1979).
6. Herbelin, J. M., and Cohen, N., "Chemical Production of Electronically Excited States in the Hydrogen-Nitrogen Difluoride System," Chem. Phys. Lett. 20, 605 (1975).
7. Lofthus, A., and Krupenie, P. H., "The Spectrum of Molecular Nitrogen," J. Phys. Chem. Ref. Data 6, 113,(1977).
8. Black, G., Slanger, T. G., St. John, G. A., and Young, R.-A., "Vacuum Ultraviolet Photolysis of Nitrous Oxide IV," J. Chem. Phys. 51, 116 (1969).
9. Husain, D., Kirsch, L. J., and Wiesenfeld, J. R., "Collisional Quenching of Electronically Excited Nitrogen Atoms by Time Resolved Atomic Absorption Spectroscopy, Faraday Disc. Chem. Soc. 53, 233 (1972).
10. Husain, D., Mitra, S. K., and Young, A. N., "Kinetic Studies of Electronically Excited Nitrogen Atoms by Attenuation of Atomic Resonance Radiation in the Vacuum Ultraviolet," J. Chem. Soc. Faraday Trans. II 70, 1721 (1974).
11. Schofield, K., "Rate Constants for Reactions of Excited Species," J. Phys. Chem. Ref. Data 8, 723 (1979).
12. Clark, W. G., and Setser, D. W., "Energy Transfer Reactions of $N_2(A^3\Sigma_u^+)$ 5. Quenching by Hydrogen Halides, Methyl Halides and Other Molecules," J. Phys. Chem. 84, 2225 (1980).

13. Hays, G. N., and Oskam, H. J., "Populations of $N_2(B^3\Pi_g)$ by $N_2(A^3\Sigma_g^+)$ During the Nitrogen Afterglow," J. Chem. Phys. 59, 1507 (1973).

14. Hays, G. N., and Oskam, H. J., "Reaction Rate Constant for $2N_2(A^3\Sigma_u^+) \rightarrow N_2(C^3\Pi_u) + N_2(X^1\Sigma_g^+, v'>0)$," J. Chem. Phys. 59, 6088 (1973).

15. Fontijn, A., Meyer, C. B., and Schiff, H. I., "Absolute Quantum Yield Measurements of the NO-O Reaction and Its Uses as Standard for Chemiluminescent Reactions," J. Chem. Phys. 40 , 64 (1964).

16. Vanpee, M., Hill, K. D., and Kineyko, W. R., "Absolute Rate Constant Measurements for the Radiative Combination of Atomic Oxygen with Nitric Oxide," AIAA J. 9, 135 (1971).

17. Golde, M. F., Roche, A. E., and Kaufman, F., "Absolute Rate Constant for the Atomic Oxygen + Nitric Oxide Chemiluminescence in the Near Infrared," J. Chem. Phys. 59, 3953 (1973).

18. Woolsey, G. A., Lee, P. H., and Slater, W. D., "Measurement of the Rate Constant for NC-O Chemiluminescence Using a Calibrated Piston Source of Light," J. Chem. Phys. 67, 1220 (1977).

19. Sutoh, M., Morioka, Y., and Nakamura, M., "Absolute Rate Constant for the Chemiluminescent Reaction of Atomic Oxygen with Nitric Oxide," J. Chem. Phys. 72, 20 (1980).

20. Clyne, M. A. A., and Thrush, B. A., "Mechanism of Chemiluminescent Combination Reactions Involving O Atoms," Proc. Roy. Soc. A269, 404 (1962).

21. Lilenfeld, H. V., and Bradburn, G. R., Private Communication (1985).

22. Rotem, A., Nadler, I., and Rosenwaks, S., "Laser Induced Fluorescence Studies of Collisional Coupling of $N_2(B^3\Pi_g)$ with $N_2(W^3\Delta_u)$ and $N_2(A^3\Sigma_u^+)$," Chem. Phys. Lett. 83, 281 (1981).

23. Sadeghi, N., and Setser, D. W., "Collisional Coupling of $N_2(B^3\Pi_g)$ and $N_2(W^3\Delta_u)$ States Studied by Laser Induced Fluorescence," Chem. Phys. Lett. 77, 304 (1981).

24. Sadeghi, N., and Setser, D. W., "Collisional Coupling and Relaxation of $N_2(B^3\Pi_g)$ and $N_2(W^3\Delta_u)$ Vibrational Levels in Argon and Neon," J. Chem. Phys. 79, 2710, (1983).

25. Benesch, W., and Fraedrich, D., "The Role of Intersystem Collisional Transfer of Excitation in The Determination of Molecular Nitrogen Vibronic Level Populations, Application to $B'^3\Sigma_u^- - B^3\Pi_g$ Band Intensity Measurements, J. Chem. Phys. 81, 5367 (1984).

26. Rotem, A., Nadler, I., and Rosenwaks, S., "Direct Observation of Collision Induced Transitions from $N_2(B^3\Pi_g)$ to $N_2(B'^3\Sigma_u^-)$," J. Chem. Phys. 76, 2109 (1982).

27. Mitchell, A. C. G., and Zemansky, M. W., Resonance Radiation and Excited Atoms, Cambridge University Press, London (1971).

28. Kaufman, F., and Parkes, D. A., "Sources of Error in Using Resonant Light Absorption to Measure Atomic Concentrations," Trans. Faraday Soc. 66, 1579 (1970).

29. Bemand, P. P., and Clyne, M. A. A., "Atomic Resonance Fluorescence Spectrometry for Rate Constants of Rapid Bimolecular Reactions 3. Oxygen Atom Resonance," J. Chem. Soc. Faraday II 69, 1643 (1973).

30. Clyne, M. A. A., and Piper, L. G., "Kinetic Spectroscopy in the Far Vac. UV. Part 3. Oscillator Strengths for Transitions in Atomic Oxygen," J. Chem. Soc. Faraday II 72, 2176 (1976).

31. Hood, R. J., and Reck, G. P., "Binary Collision Broadening. Determination of Dispersion Force," J. Chem. Phys. 56, 4053 (1972).

32. Berman, P. R., and Lamb, Jr., W. E., "Influence of Resonant and Foreign Gas Collisions on Line Shapes," Phys. Rev. A 187, 221 (1969).

33. Clyne, M. A. A., and Townsend, L. W., "Determination of Atomic Oscillator Strengths Using Resonance Absorption with a Doppler Line Source: Transitions of Br and I $(n+1)s\text{-}np^5$," J. Chem. Soc. Faraday II 70, 1863 (1974).

34. Lin, C. L., and Kaufman, F., "Reactions of Metastable Nitrogen Atoms, J. Chem. Phys. 55, 3760 (1971).

35. Fell, B., Rivas, I. V., and McFadden, D. L., "Kinetic Study of Electronically Metastable Nitrogen Atoms, $N(2^2D_J)$, By Electron Spin Resonance Absorption," J. Phys. Chem. 85, 224 (1981).

36. Clyne, M. A. A., in Physical Chemistry of Fast Reactions, (Plenum Press NY 1973), vol. 1.

37. Kaufman, F., Progr. Reaction Kinetics 1, 1 (1961).

38. Walker, R. E., "Chemical Reaction and Diffusion on a Catalytic Tubular Reactor," Phys. Fluids 4, 1211 (1961).

39. Poirier, R. V., and Carr, R. W., "Use of Tubular Flow Reactors for Kinetic Studies Over Extended Pressure Ranges," J. Phys. Chem. 75, 1593 (1971).

40. Ferguson, E. E., Feshenfeld, F. C., and Schmeltekopf, A. L., Flowing Afterglow Measurements of Ion-Neutral Reactions," Adv. At. Mol. Phys. 5, 1 (1969).

41. Farragher, T. L., "Ion Molecule Reaction Rate Studies in a Flowing Afterglow System," Trans. Faraday Soc. 66, 1411 (1970).

42. Langhaar, H. L., "Steady Flow in the Transition Lengths of a Straight Tube," Am. Soc. Mech. Eng. Trans. E64, A55 (1942).

43. Iannuzzi, M. P., and Kaufman, F., "Rates of Some Reactions of Atomic Nitrogen (^2D and ^2P) Near 300K," J. Chem. Phys. 73, 4701 (1980).

44. Slanger, T. G., Wood, B. J., and Black G., "Temperature Coefficients for $N(^2D)$ Quenching by O_2 and N_2O," J. Geophys. Res. 76, 8430 (1971).

45. Davenport, J. E., Slanger, T. G., and Black, G., "The Quenching of $N(^2D)$ by $O(^3P)$," J. Geophys. Res. 81, 12 (1976).

46. Black, G., Sharpless, R. L., Slanger, T. G., and Lorents, D. C., Quantum Yields for the Production of $O(^1S)$, $N(^2D)$ and $N_2(A^3\Sigma_u^+)$ from Vac. UV Photolysis of Nitrous Oxide," J. Chem. Phys. 62, 4266 (1975).

47. Meyer, A., Setser, D. W., and Stedman, D. H., "Energy Transfer Reactions of $N_2(A^3\Sigma_u^+)$. II. Quenching and Emission by O and N Atoms," J. Chem. Phys., 74, 2238, (1970).

48. Whitefield, P. D., and Hovis, F. E., Nitrogen Metastable A-State Kinetics Technical Proposal, Report MDC Q1217, 16 April 1984.

49. Whitefield, P. D., and Hovis, F. E., Active Nitrogen Generation, Quarterly Status Report, 10 October 1985.

50. Reactive Intermediates in the Gas Phase, Setser D. W., Editor, Chapt. 1 (Acedemic Press, London, 1979).

51. Laidler, K. J., Chemical Kinetics, 2nd. Edition, Chapt. 1, (McGraw-Hill, St. Louis, 1965).

52. Palmer, M., AFWL, private communication (1985).

53. Gordon, S., and McBride, B. J. Computer Program for Calculation of Complex Chemical Equilibrium Compositions, Rocket Performance, Incident and Reflected Shocks, and Chapman-Jouguet Detonations, Report NASA SP-273, Interim Revision 1976.

54. N_2F_4 Gas Chromatographic Analysis, TRW, January 1985.

Appendix A

The N_2F_4 Handling Facility: Development, Construction and Operation.

The timely completion of the studies described in this report required experiments, using various mixtures of N_2F_4 in He, to be performed simultaneously at any two of three independent experimental stations. Futhermore, the hazardous nature of N_2F_4 required that the source bottle and subsequent handling of the undiluted gas be located and operated remotely from the experimental stations. These requirements were met by the design and construction of the MDRL N_2F_4-Handling Facility. This facility is essential to the contract; however, its construction and material costs were funded by MDRL because it enhances experimental capabilities for related IRAD projects. Contract funds for this facility were expended in design labor hours associated with the specific needs of handling N_2F_4 in this facility.

The N_2F_4 handling facility consists of a metal cabinet connected to the outside of the building through a stack fitted with a blower. The blower creates a constant flow of air through the cabinet to the outside. Inside the cabinet are two stainless steel accumulators with a capacity of ~40 ℓ each. A remotely actuated preparation line facilitates the delivery of N_2F_4 and diluent gases to the accumulators, and similarly remotely actuated delivery lines bring the prepared and equilibrated mixtures to the experimental stations.

To minimize the possibility of mixture contamination from an incorrect valve opening, a master control panel has been designed and constructed. Incorporating solid-state logic circuitry, the control panel is programmed to prepare for the automatic opening of a sequence of valves to perform a specific predetermined function and to display this sequence preparation on the control panel. Motor-driven metering valves control the flow of gases to the accumulators and can be manually preset at this stage. After the correct sequence is chosen, all the required valves can be operated simultaneously by setting one master sequence switch.

In the unlikely event of a dangerous situation at either of the experimental stations using the facility, or at the handling facility itself, the entire system can be placed into a standby mode by activating an abort switch

at either of the experimental stations (the master control panel for mixture preparation is located at one of the experimental stations). In the standby, mode all the valves are automatically shut, but their condition at the time of the abort remains indicated on the master control panel. This assists in subsequent trouble shooting. The preparation line is fitted with a diffusion-pumping capability and all necessary pressure monitors. In an emergency the entire system can be vented and purged through a heated charcoal scrubber which is, in turn, vented through the stack.

END

11-87

DTIC